3 1293 01055 3315

This is to certify that the

thesis entitled

The Adhesion of Ion Beam Irradiated
Ultra-High Molecular Weight Fibers to
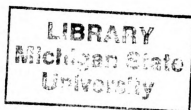Epoxy Matrix
presented by

Richard Schalek

has been accepted towards fulfillment
of the requirements for

Master's degree in Materials Science

Major professor

Date 2-28-92

PLACE IN RETURN BOX to remove this checkout from your record.
TO AVOID FINES return on or before date due.

DATE DUE	DATE DUE	DATE DUE
FEB 03 2001		

MSU Is An Affirmative Action/Equal Opportunity Institution

THE ADHESION OF ION BEAM IRRADIATED ULTRA-HIGH MOLECULAR WEIGHT POLYETHYLENE FIBERS TO EPOXY MATRICES

By

Richard Lee Schalek

A DISSERTATION

Submitted to
Michigan State University
in partial fulfillment of the requirements
for the degree of

MASTER OF SCIENCE

Department of Materials Science
and Mechanics

1992

ABSTRACT

The Adhesion of Ion Beam Irradiated Ultra-High Molecular Weight Polyethylene Fibers to Epoxy Matrices

By

Richard Lee Schalek

Ultra-high molecular weight polyethylene (UHMW-PE) fibers have a highly chain-extended and crystalline structure which is functionally inert and requires surface modification before it can operate as a reinforcement in polymer matrix composites. Traditional fiber surface techniques provide adequate fiber-matrix adhesion, but also degrade the fiber's mechanical properties. Low energy (100 to 1000 eV) ion irradiation is an emerging material surface modification technique. UHMW-PE Spectra-1000 fibers were irradiated by high (>30 keV) and low energy ions to doses of 1×10^{13} cm^{-2} to 1×10^{17} cm^{-2}. Interfacial shear strength (ISS) tests show a maximum increase of 900%, with little loss in tensile strength for the low energy irradiations. The responsible adhesion mechanisms were the improved wetting properties, due to surface oxidation, and increased fiber-matrix mechanical interlocking. The achievable ISS is dependent on the tailored fiber surface microstructure and the cohesive strength of the fiber.

Table of Contents

LIST OF TABLES

LIST OF FIGURES

Chapter One
INTRODUCTION

The development of high performance organic reinforcing fibers has lead to significant advances in the area of structural composites. Organic fibers typically display tensile strengths and tensile modulii of 4 GPa and 200 GPa, respectively. This matches the tensile performance of metal and glass fibers when compared on an absolute scale, while surpassing them when compared on a weight-to-strength basis.

The effectiveness of the load transfer from the brittle matrix to the fiber, via the fiber-matrix interphase, often is the limiting factor in the success or failure of a structural composite. A fundamental understanding of fiber-matrix adhesion in different composite systems is therefore a first step in realizing the potential of these high performance organic reinforcing fibers.

High performance organic fibers can be divided into three major classes: graphite fibers, synthetic rigid polymer fibers, and fibers of chain-extended, flexible polymers. Only graphite and synthetic rigid polymer fibers have found commercial success as reinforcing agents in structural composites. The commercial use of chain-extended flexible polymers (comprised of only highly oriented polyethylene) in structural composites has been limited by their relatively low adhesion level to epoxy matrices. The poor interfacial bonding results from the chain extended crystalline morphology of the fiber combined with the lack of chemically active sites on the polymer backbone. The poor adhesive properties of polyethylene fibers have limited their use to composites for ballistic applications where energy intensive absorption by fiber-matrix delamination is the primary goal.

The adhesion of polyethylene fibers to polymeric matrices is commonly improved by some type of fiber surface treatment, such as plasma, corona or chemical processes, with plasma treatments being the most successful, economical and the most widely studied [1, 2, 3, 4]. These surface modification processes are designed to control the chemical
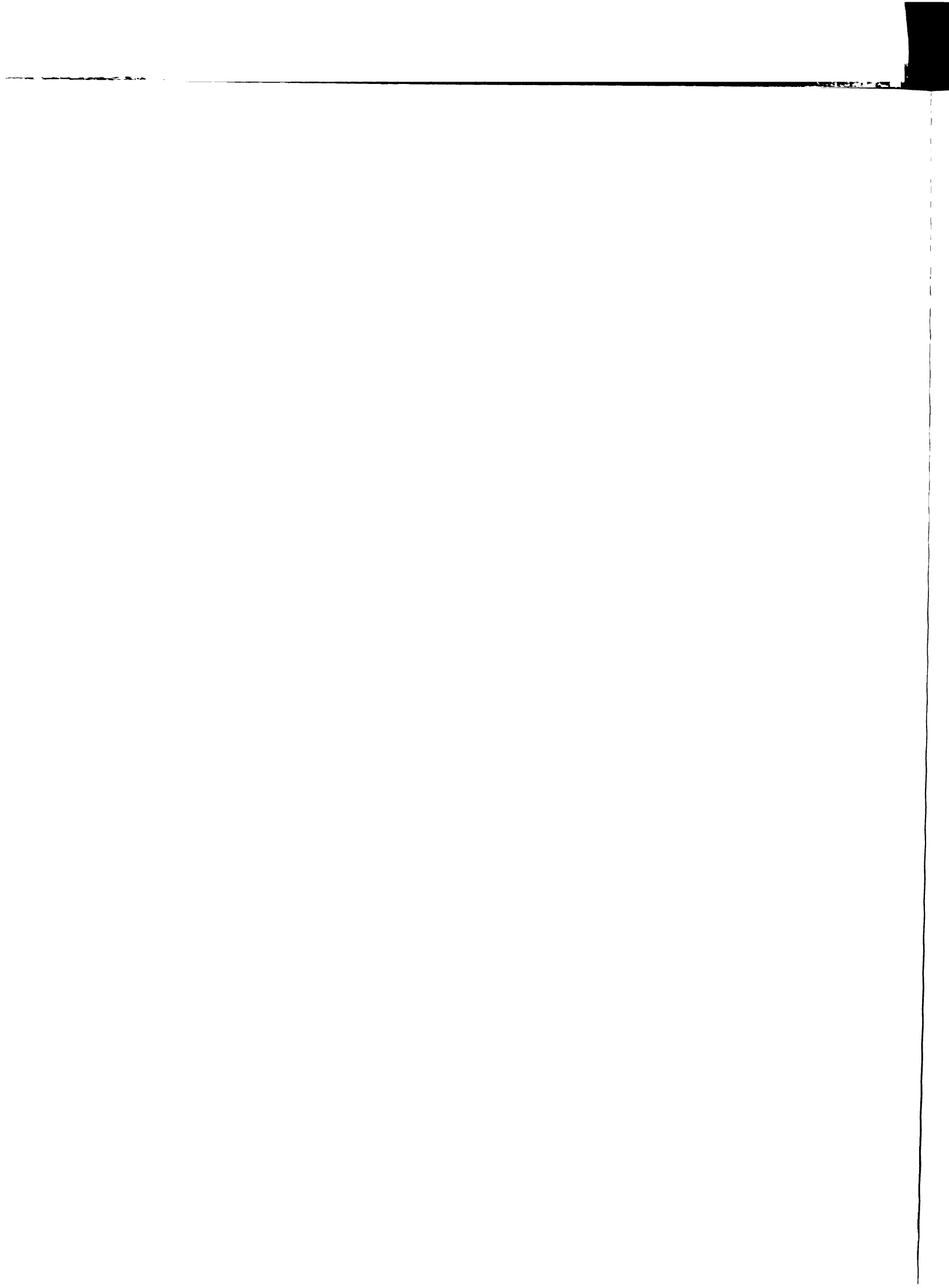
surface functionality, alter surface topography and/or to remove weak boundary layers containing low molecular weight oligomers or other additives, with the general objective of improving adhesion and wettability of the fiber surface.

Many fiber surface treatments have met with success; however, the techniques are highly parameter-sensitive and often negatively affect bulk fiber properties. Improved surface processing methods are therefore actively sought. Low energy broad-beam ion processing is a rapidly developing materials modification technology which complements and has several distinct advantages over the more traditional fiber surface altering techniques [5]. Precise control of experimental parameters, such as ion direction, energy, flux and background pressure are currently not available from other processes. This increased experimental parameter control capability allows a more direct correlation between the observed surface modifications and fundamental ion-solid interactions, than is available from traditional surface modification techniques.

As a separate issue from surface modification of polymers for adhesion enhancement, there has been increasing interest in studying ion beam interactions with polymeric and insulating materials. Compared to metals and semiconductors, polymers have distinct radiation damage mechanisms arising primarily from the differences in molecular structure and chemistry. Bombardment by energetic ions causes the polymer components within the depth of ion penetration to interact with the incident particle, forming ionized stable and metastable radicals which subsequently thermalize and recombine or leave the surface resulting in substantial surface modification. The extent to which these radiation effects alter the polymer properties depends on the chemistry and structure of the polymer as well as the nature of the ion beam, particularly the ion type, energy and dose.

Within the past 20 years low energy broad-beam ion sources have become important surface modification devices. The technological development of these low energy ion sources originated in the program for electric space propulsion [6, 7]. Significant use

of gridded, broad beam ion sources started about 1970 and increased thereafter. At present, these ion sources are available in diameters of 1 cm to 38 cm, with ion-beam currents ranging from a few milliamperes to several Amperes.

The large current capability of a broad-beam ion source results in substantial processing capacities and, hence, is useful in industrial applications. In a gridded source, the large currents are made possible with optics that allow the beam profile to be focussed or defocussed (diverging). Thus, the ions are accelerated into a beam with a well-defined and controlled direction, density and energy. These experimental characteristics simplify the control and process definition for ion beam sources over that of the competitive plasma processes.

The present study is a continuation and expansion of a previous investigation initiated by Ozzello, et al. [8] concerning the effects of high energy (30-135 keV) ion implantation of Spectra 1000 UHMW-PE fibers. Ozzello, et al. [8] found that high energy ion irradiation resulted in a 300% increase of the fiber-matrix interfacial shear strength (ISS), with little, if any, degradation of the fiber tensile strength. These results provided the impetus for the current study that investigates the mechanisms responsible for the observed increases in ISS in both high energy and low energy (100 - 1000 eV) ion implantations.

Tensile strength and ISS experiments determined the effects of low energy ion irradiation on the mechanical properties of the fibers. Surface chemistry characterization (x-ray photoelectron spectroscopy (XPS), Fourier transform infrared spectroscopy (FTIR)) of both the high and low energy ion irradiated fibers have been performed, followed by physico-chemical characterization using surface energy and gel-fraction techniques.

Chapter Two presents a review of the literature including discussions of the general concepts of adhesion, a description of the method of producing UHMW-PE fibers along with a summary of physical and mechanical property data of Spectra -1000 fibers. A summary of traditional fiber surface modification techniques currently used to enhance

fiber-matrix adhesion is presented. The general effects of high and low energy ion implantation of polymers and their relevance to fiber-matrix adhesion are discussed. Chapter Three discusses sample preparation, surface chemistry characterization techniques and experimental methods for determining mechanical properties. Chapter 4 presents and discusses the experimental results . Chapter 5 draws conclusions regarding the probable adhesion enhancement mechanisms and their contributions.

Chapter Two
REVIEW OF THE LITERATURE

The Composite Interphase

The concept of the interphase has been described as the region existing between the bulk fiber and the bulk matrix [9]. The interphase region, shown in Figure 2-1, presumably consists of unreacted species, impurities, voids and the fiber surface morphology resulting in thermal, mechanical and chemical environments that are different from that of the bulk matrix and reinforcing phase. The effective bonding between the fiber and matrix is thus complicated, requiring both chemical and mechanical characterization to completely understand the underlying adhesion mechanisms.

The physical and mechanical properties of a composite depend to a great extent on the structure and properties of the fiber-matrix interphase; therefore, the adhesive bond between the fiber and matrix is of prime importance to the performance of composite materials. This interphase bond is not only significant to the strength and stiffness of the composite (particularly off-axis), but also governs mechanisms of damage accumulation and propagation.

The adhesion of the fiber to the matrix can be attributed to adsorption and wetting, interdiffusion, electrostatic attraction, and mechanical interlocking mechanisms [10, 11]. These mechanisms are complex combinations of chemical and physical interactions. Adsorption is the molecular attraction and collection of one molecular species onto the surface of another and results either through chemical interactions or physisorption interactions. In general, chemical bonding interactions are two orders of magnitude greater in strength than physisorption interactions and, hence, more desirable. Physisorption mechanisms include nonpolar (Van der Waals) and polar (dipole and acid/base) interactions, which, though weaker, act over longer distances.

Epoxy Matrix

Fiber

Interphase

Epoxy Matrix

Polymer of Different Properties

Unpolymerized Resin

Voids

Impurities

Modified Fiber Surface
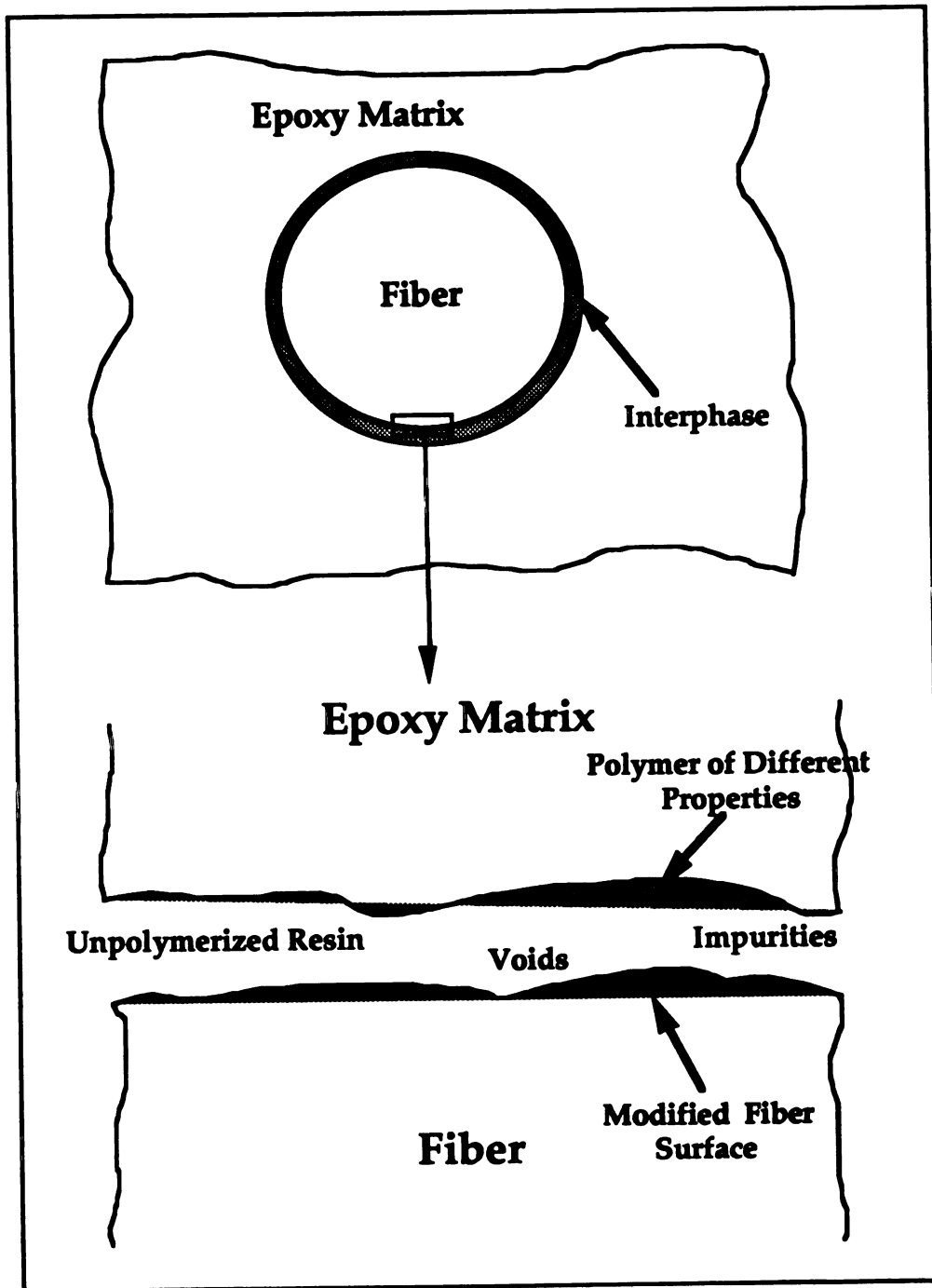
Fiber

Figure 2-1: Illustration of the three dimensional interphase.

The production of fiber reinforced polymeric composites requires that a liquid resin make close contact with the surface of the fiber. An intimate fiber-resin interface is formed when the liquid resin completely spreads onto, or wets, the solid surface. Poor wetting of the fibers results in voids between the fiber and the solidified matrix, decreasing the ultimate strength of the composite. Maximizing the interfacial molecular adhesion between the fiber and the liquid resin, by matching the surface energy components of the two adhering phases, maximizes the amount of fiber-matrix wetting.

Though wetting does not directly affect bonding mechanisms, it is a prerequisite to achieving maximum levels of fiber-matrix adhesion. For a general fiber-matrix system, a criterion for adequate wetting is difficult to define. Operational definitions, based on thermodynamic considerations, provide a convenient method of expressing the relative degree of fiber-matrix wetting. For instance, good wetting can be defined as the spreading of a liquid on the surface of a solid with the fiber-resin contact angle less than 90 degrees. Also, if the surface energy of the fiber is greater than that of the resin adequate wetting will occur.

Molecular interdiffusion is another possible fiber-matrix adhesion mechanism. The bond strength depends on the amount of molecular entanglement, the number of molecules involved and the strength of the bonding between the molecules. For most polymers, interdiffusion between the epoxy and fiber is limited, but in the case of UHMW-PE, where the composite consolidation temperature is approximately 85% of the melting temperature, interdiffusion may occur, resulting in enhanced adhesion.

Differences in the electrostatic charge between the fiber and the resin matrix, resulting from the transfer of electrons across the interface, may also contribute to attractive forces which bond the fiber to the resin. For polymers, these electrostatic attractive forces are usually small when compared to other interactions and can probably be neglected for most fiber-matrix systems.

Lastly, mechanical interlocking between the fiber and matrix may substantially increase adhesion by maximizing the fiber-matrix contact area and providing more possibilities for chemical interactions and additional frictional resistance to shear stresses. Increased fiber surface roughening, induced by fiber surface modification, increases the amount of mechanical interlocking and adhesion. Adequate wetting, combined with the minimization of voids, must be achieved or maximization of fiber-matrix adhesion will be compromised. Furthermore, surface pits associated with surface roughening act as stress concentrators and degrade the mechanical properties of the fiber.

In addition to these mechanisms, the fiber-matrix coefficient of thermal expansion mismatch can create residual stresses and cracks during cool-down after composite processing degrading fiber-matrix interfacial properties. Weak boundary layers (WBLs) consist of impurities and low molecular weight oligomers on the fiber surface. WBLs have lower cohesive or adhesive properties than their bulk substrates and serve as weak interfacial links. Removal or strengthening of WBLs is beneficial to achieving high levels of adhesion.

The interfacial shear strength (ISS) characterizes the adhesion of the fiber-matrix interphase. The three most common methods for determining the ISS are the single fiber fragmentation technique [12,13], the microdroplet pull-off technique [14,15] and the *in-situ* microindentation technique [16]. For the case of UHMW-PE fibers, the strain to failure of the fiber is too high to be tested in the single fiber fragmentation test. Furthermore, the inherent polishing difficulties of polyethylene fibers, combined with the fiber's viscoelastic nature, discourages the use of the microindentation technique. The microdroplet pull-off technique is therefore the appropriate test for UHMW-PE fibers.

Studies by Herrera-Franco et al [17] and Drzal and Herrera-Franco [18] analyzed and compared these techniques. They show that loading conditions of the microdroplet may affect the interfacial stress distribution in the case of the microdroplet pull-off technique. Furthermore, differences in the shape of the droplet meniscus and the length of

the fiber supporting the droplet on the interfacial stresses help explain the frequently observed scatter of experimental results. Also, Gaur and Miller have investigated the microdroplet pull-off experimental parameter effects on the interfacial shear strength of Kevlar, glass and carbon fibers [19]. Their results indicate that the shear strength decreases with increasing fiber-matrix interfacial area length and that there is no significant load rate effect on shear strength.

Ultra-High Molecular Weight Polyethylene Fibers

A ultra-high molecular weight polymer combined with a high degree of crystalline chain orientation results in the achievement of high strength and high modulus fibers. For polyethylene fibers, producing both ultra-high molecular weight and a high degree of chain orientation is difficult since the extremely long, flexible, chain polymer tends to tangle in the melt.

To reduce the number of entanglements and increase the chain extension in UHMW-PE fibers, a unique drawing method developed by Cappaccio and Ward [20] is currently used as a general production technique. This gel spinning process uses ultra-high molecular weight polymers dissolved in a solvent which disentangles the polymer chains. This network is then drawn in an oven to high draw ratios (λ>>20) where molecular chains are transformed from a folded-chain conformation into a nearly extended-chain conformation as shown in Figure 2-2. The quenching of the extrudate leads to the formation of a gel fiber from which the solvent is either evaporated or extracted by a second, low melting point solvent. General reviews of this process and a solid state extrusion method are given by references [21,22]. The current trade names and producers of polyethylene fibers are: Spectra (Allied-Signal Corp., Petersburg, VA), Celanese (Celanese Research, New Jersey), Snia (Snia Fibre, Milan, Italy) and Tekmilon (Mitsui Petrochemicals Ltd., Tokyo, Japan). Table 2-1 compares some mechanical properties of Spectra-1000 fibers with those of Kevlar 49.

Conventional Fiber

- Relatively low molecular weight
- Moderate oreintation
- Crystalline regions chain folded

Extended-chain fiber

- Very high molecular weight
- Very high degree of orientation
- Minimum chain folding
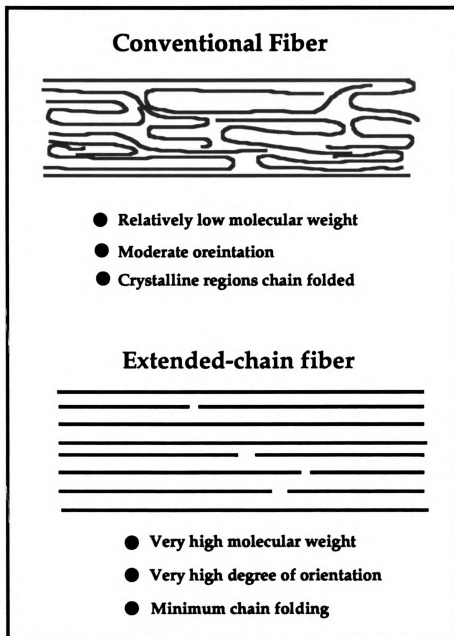
Figure 2-2: Schematic representation of conventional polyethylene
fibers and chain-extended polyethylene fibers.

The supermolecular structure of UHMW-PE fibers consists of either a shish-kebab morphology or smooth microfibrillar morphology. Recently, Hofmann, et al. [23] investigated, via transmission electron microscopy, the fiber surface morphology of Spectra 900 and Tekmilon using a two-stage replica sample preparation technique. The TEM micrographs reveal that the Spectra fibers were mainly composed of smooth microfibrils with negligible lamellar overgrowth. In contrast, the Tekmilon fiber had a distinct shish-kebab structure. The smooth microfibrils observed in the Spectra were believed to be a result of the high degree of drawing resulting in the unfolding of lamellar crystallized molecular ends.

The segregation of impurities and low molecular weight species to the fiber surface during fiber manufacturing produce WBLs. Several investigators have studied the effects of molecular processes and impurity effects on the mechanical properties of the UHMW-PE fibers. For instance, Kalb and Pennings [24, 25] investigated the influence of the microporosity and maximum strength of high molecular weight polyethylene fibers on the drawing process and concluded that drawability of polymer fibers is influenced by the mobility of the polymer molecules. Inhomogeneities inherent in the fibers included variations in the fiber diameter, polymer concentration and orientation, and the inclusion of segregated impurities acquired during the spinning process.

Barham and Keller [26] systematically studied the crystallization conditions and drawing conditions of polyethylene fibers. They used single crystal mats of PE and found that the most stringent condition for achieving high moduli was the minimization of low molecular weight species inherent in the starting material. They also found that impurities, in segregated form, were required to maximize the draw ratio. Thus, to produce fibers with optimal mechanical properties, strict control over the nature and amount of low molecular weight species is essential.

Table 2-1: Mechanical properties of Spectra-1000 and Kevlar-49 fibers.

Fiber	Modulus GPa	Tensile Str. GPa	Density g/cm^3	Comp. Str. GPa	T_m °C
Spectra 1000	170	3.0	0.97	0.17	147
Kevlar 49	125	3.4	1.47	0.39-0.48	—

Fiber Diameter = 30 µm

$M_w = 10^6$

Traditional Surface Treatments

Plasma and Chemical Treatments   Traditional methods for altering the surface and near-surface properties of polymers and, in particular, UHMW-PE fibers include chemical, corona and plasma treatments. All have met with varying degrees of success, but the overwhelming method of choice, with economical feasibility and adhesion improvement, is plasma treatment. These methods modify the polymer surface in similar ways. Since the physical processes occurring during plasma treatment are closely related to those of ion implantation, most of the literature review focuses on plasma treatments.

Liston [27] recently published a review article on the influence of low-pressure glow-discharge plasmas on the surface properties of polymers, and a description of the necessary equipment for plasma production. Though he does address the issue of the bonding characteristics of the treated polymers to other materials, he does not specifically treat the issue of adhesion between polymer fibers and epoxy matrices. The two major physical effects of plasma surface treatment of polymers are microablation and surface cleaning. Crosslinking, or chain scission, and surface activation are the result of chemical processes occurring in the polymer during plasma processing. The predominance of one process over the other is manipulated by varying the process conditions.

Microablation denotes removal of the host material, whereas cleaning is the removal of an unbound layer of contamination. Microablation and surface cleaning both remove organic material by volatilizing low molecular weight hydrocarbons formed from either oxidative or other free radical induced degradation reactions. For crystalline polymers the ablation rate differs between the amorphous and the crystalline regions, resulting in a preferentially etched surface.

A study by Holmes and Schwartz [28] investigates the plasma treatment of ultra-high strength polyethylene (Spectra 900) fabric using an ammonia gas to attach surface amine groups. Water contact angles decreased to zero after only 5 minutes in the plasma,

rendering the fabric surface completely wettable. The addition of primary and secondary amine groups to the fiber surface increased the wetting. They also measured a 10% reduction in fiber tensile strength.

The tensile strength and the modulus of UHMW-PE fibers increases as the draw ratio increases. Ladizesky and Ward [29, 30] have extensively studied the effects of chemical acid and plasma treatments on the adhesion of UHMW-PE fibers to epoxy matrices on different draw ratio fibers. They found the acid treatment is most effective for the intermediate draw ratio material, whereas the plasma treatment is most effective for the higher draw ratio fibers. The maximum pull-out adhesion was found to be 4.9 MPa (a 100% increase over the untreated fibers), but at the expense of a 42% decrease in tensile strength. Scanning electron micrographs indicated a cellular structure on the fiber surface, with the pit size increasing with increasing draw ratio, accompanied by a decrease and even disappearance of the fibrillated surface. They assert that the pull-out failure occurred by peeling-off of the filaments and took place in two stages, namely initiation and propagation of the fracture.

A microdroplet technique was used to determine the interfacial shear strength [31] of plasma surface modified UHMW-PE Spectra 1000 fibers. An SEM investigation of the fiber surface indicated that uniform cellular microcavitation of the Spectra fibers occurred. The interfacial shear strengths of the Spectra fibers increased for all the plasma treatments irrespective of the chemical nature of the ionized gas. They hypothesized that texturing of the fiber surface improved the adhesive bond strength.

A recent study by Tissington, et al. [32] investigated the effects of oxygen plasma treatments on the mechanical properties of different types of ultra-high strength polyethylene fiber composites. They found that the interlaminar shear strength increased (79%) by pretreating the reinforcement with an oxygen plasma. Composite mechanical properties such as tensile strength and modulus and the ultimate flexural strength and flexural modulus were shown to be largely independent of the plasma treatment.

Other investigators [33] studied the effects of surface fluorination on the adhesion of Spectra 1000 fibers to epoxy matrices. Contact angles determined the wettability of the fibers, while XPS and infrared spectroscopy elucidated the surface chemistry. The increase in fiber surface wettability, along with surface roughening, contributed to the 400% increase in interfacial shear strength. The role of the oxygen incorporation during fluorination on chemical bonding needs further study.

Electron and Photon Irradiation   Other treatments, such as electron and photon irradiation do not directly improve fiber-matrix adhesion, but improve the mechanical properties of UHMW-PE fibers. A series of studies by Chen and Ranby [34, 35, 36] details the effects of photocrosslinking on the mechanical properties, high temperature resistance and creep behavior of Spectra 900. No appreciable changes in tensile strength or modulus appeared for fibers with a gel content of up to 91% at room temperature.

Klein, et al. [37] studied the structure and properties of electron irradiated UHMW-PE filaments before drawing as a function of irradiation dose in an attempt to decrease the creep rate of the drawn fibers. Gel content, differential scanning calorimetry, elasticity and x-ray measurements, along with creep measurements, indicated that extensive chain branching and formation of a permanent network occurred as a result of the irradiation. The tensile creep rate is decreased by four orders of magnitude and is described well in terms of two thermally activated processes, one crystalline and one amorphous, acting in parallel.

Ion Implantation of Polymers

General Considerations   Ion implantation is the introduction of dopants (impurities or alloying elements) into the surface layers of solids by energetic ion beams. Stopping of these energetic ions involves the production of a tremendous amount of damage (vacancies,

interstitials and amorphization) by collisional processes and bond breakage. The induced damage alters the chemical, electrical and mechanical properties of the host materials in beneficial ways. To date, the effects of ion implantation on all classes of materials (i.e., metals, semiconductors, and insulators) have been studied [38, 39]. The ion implantation of polymeric materials, a subset of the insulator class, has only recently (within the past 15 years) been aggressively investigated, due primarily to their importance in the electronics industry. Several review articles concerning ion implantation of polymers have recently been published [40,41].

The energy deposited from the incoming ions to the target accounts for most of the phenomena observed during and after ion bombardment of polymers. The energy loss is phenomenologically partitioned into electronic interactions (ionization and excitation of the host material atoms) and nuclear (hard sphere) interactions. The process by which a particle loses energy when it moves through a medium consists of a random sequence of independent events between the moving projectile and an electron or nucleus attached to an atom of the solid. For a target that contains more than one element, the energy loss is the sum of the losses of the constituent elements weighted by the abundance of elements. The probability of interaction between the incident ion and the atom of the solid is described by the stopping energy cross section, ε.

The energy loss of an incident ion can then be characterized by Bragg's rule (Equation 2-1) for the stopping power cross section[40].

$$\varepsilon(polymer) = n\varepsilon(H) + m\varepsilon(C) + \dots \qquad 2\text{-}1$$

where n and m are the number of H and C atoms in the monomer and $\varepsilon(H)$ is the stopping power cross section for hydrogen atoms, and $\varepsilon(C)$ is the stopping power cross section for carbon atoms. Bragg's rule allows the energy loss, dE/dx (eV/A), of the accelerated ion to be written in terms of the energy deposition per unit length along the ion track,

$$dE/dx = \rho N_a \varepsilon / P_M \qquad 2\text{-}2$$

where N_a is Avogadros number, ρ is the mass density (gm/cm^3) and P_M is the molecular

weight of the monomer. The depth distribution of energy loss along the ion path is

variable, with the maximum value of the energy loss parameter, dE/dx, appearing at the end

of the ion path where the ion velocity is quite low.

The large amount of energy lost at the end of the ion travel results in a significant

quantity of atomic displacements and radiation damage. Electronic interactions produce

intense chemical effects within the irradiated polymer, while nuclear interactions produce

point and linear defects.

Other useful parameters used in the analysis of implanted polymers are the total ion

range, defined as the length of the ion track, and the projected ion range, which is the

length of the ion track perpendicular to the target surface. In the majority of ion

implantation studies, the projected ion range is the parameter of interest, since it determines

the lateral region of surface modification. The number of ions striking the target per unit

area is defined to be the ion dose.

The energy lost by the ions during the process of slowing down results in the

formation of excited states (free radicals), metastable molecular states and an ensemble of

other smaller molecules, many of which may be volatile. This process is fast ($<10^{-13}$ s)

when compared to chemical reactions ($\sim 10^{-6}$ s). Strong gas evolution (molecular emission

or sputtering) during ion bombardment has been detected in almost all of the analyzed

polymeric films. Most of the ejected particles are small neutral molecules such as hydrogen

or acetylene with other detectable ionized species about two orders of magnitude lower in

concentration [40]. This irreversible radiation damage cannot be annealed out since most

polymers are unstable at high temperatures.

Puglisi [42] classifies the modifications induced by high energy ion bombardment

into reactions giving products which do not contain the projectile and reactions between

projectile and target molecules, giving products which incorporate the projectile. The

end-of-track reactions occur when the projectile energy is about 20 eV, while the reactions producing products not containing the projectile are present all along the ion track.

Puglisi also divided the ion dose into high dose ($>10^{14}$ cm^{-2}) and low dose (< 10^{13} cm^{-2}) regimes. In the high dose regime, the bombardment of polymeric materials produces amorphous carbonaceous material almost independent of the nature of the starting material. The progressive loss of volatile species and the continuous bond rearrangement under ion bombardment induces the formation of stable carbon structures (amorphous hydrogenated carbon). As a first approximation, at high doses, the target loses memory of its original structure and stoichiometry.

In the low dose regime, the overlap between ion tracks can be neglected and the correlation between the energy input parameters, the molecular parameters of the target and the observed phenomenology becomes clearer, allowing basic ion-solid research to be performed.

Recent studies indicate that increasing the ion energy to a few keV generally enhances radiation damage effects without significantly changing the products [43, 44]. These studies also suggest that ion energies in the range of 500 to a few keV, produce near-surface chemical products similar to those produced by 100 keV ions. Furthermore, since ion energies in typical reactive plasmas range from a few eV's to several hundred eV's, similar fiber surface modification effects by high and low energy irradiations are expected.

As a group, the physical and chemical changes present in ion implanted polymers influence and/or modify the polymer stoichiometry, molecular weight and polymer solubility. Molecular emission occurs for all irradiated polymers and many times has a profound effect on the polymer stoichiometry [40]. For instance, most ion irradiated polymers show large reductions in hydrogen concentration, with reductions up to 80% detected for ion doses in the range of 10^{13} to 10^{15} cm^{-2}, for heavy and light ions, respectively. Other non-carbon elemental constituents of the polymers, such as oxygen, fluorine and chlorine behave similarly. No large amounts of sputtered carbon have been

observed. For the particular case of polyethylene, the molecular emission that occurs during ion irradiation contains the species H_2, CH_4, C_2H_2 and C_3H_5 [40].

Bond breakage and reformation during ion energy deposition induces chemical changes, resulting in crosslinking or chain scission of the polymer backbone. Though chain scission and crosslinking may both take place during ion bombardment, one process usually dominates. The crosslinking process results in molecular weight increases and the formation of a three dimensional network between the main chains. Chain scission, on the other hand, results in molecular weight decrease with increasing ion dose as shown in Figure 2-3. Polymers with a low heat of polymerization and high monomer yield during pyrolysis tend toward chain scission processes during irradiation, while crosslinking occurs in polymers with high heat of polymerization and low monomer yield [40]. Since the heat of polymerization for polyethylene is 22 Kcal/mol and the monomer yield on pyrolysis is 0.025 [40], crosslinking reactions dominate during the irradiation of polyethylene.

Since polymers are formed from many thousands or millions of monomer units, small numbers of bond changes, produced at relatively low doses (10^{13} to 10^{15} cm^{-2}), are enough to considerably modify the polymer viscosity or solubility. In general, crosslinking decreases polymer solubility, while chain scission increases the polymer solubility. For UHMW-PE, which has low solubility in most solvents, the irradiation induced crosslinking increases the solubility making the polymer more environmentally stable and heat resistant.

Examples of Irradiated Polymer Studies   The study of ion-polymer interactions provides insight into the physical and chemical irradiation induced effects which influence fiber-matrix adhesion. Recent reviews [45, 46] examine the ion-beam degradative processes occurring during irradiation. The cause of these processes are not well understood [47, 48].

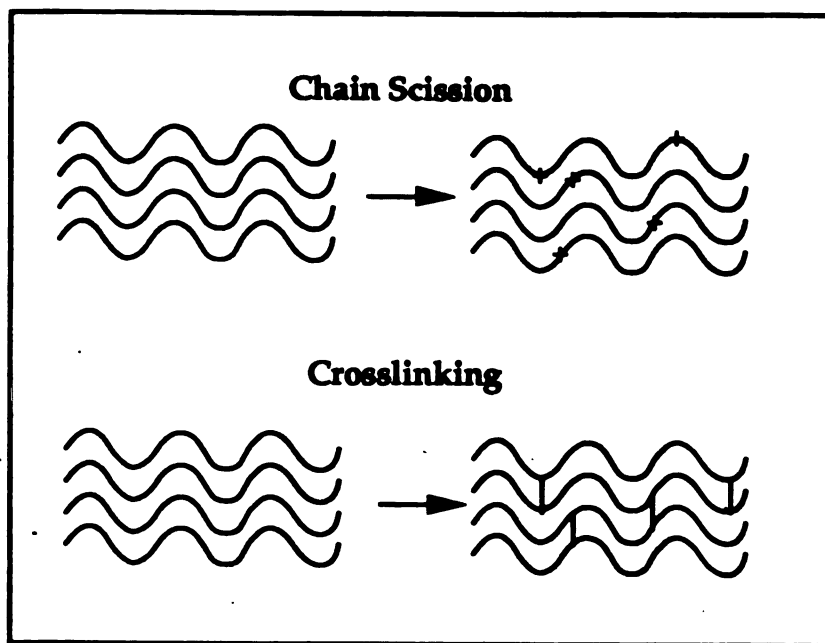**Chain Scission**
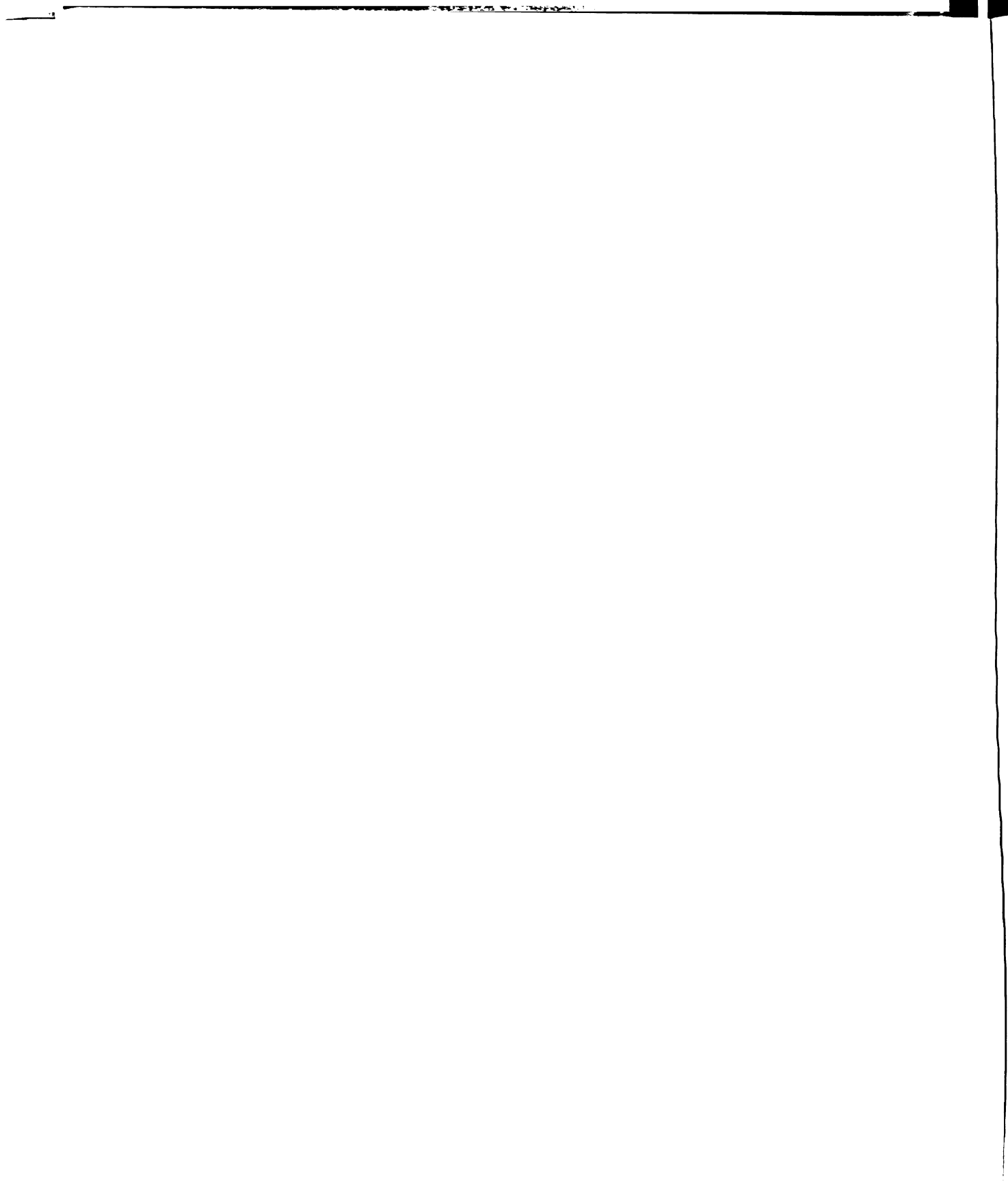
Crosslinking

Figure 2-3: Schematic illustration of chain scission and crosslinking of polymeric fibers.

Koul, et al. [49] studied the energy transfer mechanisms and the radiation chemistry of noble gas ion irradiated polymer films (Kapton, Teflon, mylar, cellulose nitrate, and CR-39). Studies as a function of ion energy and dose elucidated the chemical and physical effects of the irradiation. SEM micrographs suggested that, in these polymers, the gas atoms form bubbles by coalescence, leading to stress and cracking after prolonged irradiations.

For He ions in Teflon, cracking developed at doses near 3×10^{14} cm^{-2}. In contrast, for Ar ions in Teflon, the critical dose is two orders of magnitude higher. Also, they observed that the irradiation induced surface topography depends primarily on the radiation sensitivity of the polymer. They concluded that, for Teflon, basic electronic energy transfer mechanisms are responsible for the development of the surface topography, quite in contrast to Kapton where nuclear mechanisms seem to dominate.

The modification of polymers by ion irradiation occurs predominantly in the region of the ion's implant depth. Studies of ion range profiles in irradiated polymers indicates discrepancies between the theoretically predicted ion range and the experimentally observed results. In one study by Fink, et al. [50] the depth profiles of light ions (Li, B and Fl) implanted into organic polymer films were investigated. They found that, at a certain threshold implantation energy, there is a transition from a regular ion profile (as predicted by TRIM [51]) to an irregular one. This transition occurs whenever the electronic stopping power starts to dominate the energy transfer process. They note that the variation in the implanted dose did not affect either the range distribution parameters or the profile shapes. This occurs even though, at doses above 1×10^{15} cm^{-2}, polymers exhibit drastic changes in their compositions.

Systematic measurements were carried out on the optical absorption depth profile, and the particle mass and dose dependence of the optical absorption. They show that the blackening profile resembles the vacancy profile and not the profile of the electronic energy

transfer (ionization profile). This suggests that the discoloration results from nuclear interactions.

Ion irradiation of polymers also affects the surface mechanical properties either through crosslinking or chain scission reactions. Lee, et al. [52,53] measured the irradiation induced hardness changes of several different polymers (Kapton, Teflon, and Mylar). Residual gas analysis during irradiation identified the liberated gases as mostly hydrogen, carbon monoxide, carbon dioxide, acetylene and hydro-fluorocarbons. Teflon suffered the most decomposition, as evidenced by the largest pressure increase during irradiation. Substantial increases in the nanoindentation hardness of all the irradiated polymers were found, with Kapton having a hardness 3 times that Fe-Cr-Ni stainless steel. They assert that the irradiation induced three dimensional crosslinking state increased the surface hardness of the polymer. The implanted materials also had lower wear rates than unirradiated polymers. In general, higher outgassing rates resulted in lower hardness values and higher wear rates.

Ion implantation of polyethylene has been investigated by several groups. For instance, Ishitani, et al. [54] used various analytical techniques (SIMS, FTIR, Raman and ESR) to characterize oxygen implanted polyethylene. Depth profiling by SIMS shows a monotonically decreasing oxygen content for an ion energy of 80 keV at a dose of 5×10^{14} cm^{-2} that, they suggest, results from the diffusion of the implanted oxygen out of the polymer. In contrast, 5×10^{16} cm^{-2} irradiated samples had the distribution predicted by projected range theory. They identified hydroxyl, carbonyl, acid anhydride and unsaturated hydrocarbons, including aromatic rings, on the polymer surface. The relative amount of aromatic structure increased with dose, whereas the other functional groups decreased with dose after reaching a critical dose. This correlates well with the monotonic increase of amorphous carbon as detected by Raman spectroscopy. The depth profile of the generated functional groups indicated bound oxygen in the modified layer as oxygen containing organic compounds.

Oxygen-implanted polyethylene had a high carbon radical concentration, (on the order of 1×10^{15} spins/cm^2) which saturated at a dose of approximately 1×10^{16} cm^{-2}. Aliphatic free radicals formed in the beginning of the irradiation were unstable, but the conjugated structure stabilized over a period of several months.

Schaible, et al. [55] also studied the induced chemical changes and dielectric properties of polyethylene irradiated by high energy ion implantation. At doses above 3×10^{15} cm^{-2}, no appreciable increase in the number of free radicals occurs, even though ions are continually being implanted. The stabilization of the free radical concentration at a certain dose level indicated that either no new free radicals were being formed or new free radicals react with the free radicals already present resulting in an equilibrium free radical concentration. The dose rate had no effect on the free radical concentration.

They also found that higher doses of O$^+$ ions irradiations were required to generate the same concentration of free radicals as Ar$^+$ ions. This is consistent with the fact that heavier ions generate more damage in the polymer than lighter ions. Increasing the temperature of the sample during irradiation results in enhanced radical formation. This can be conceptually understood since at lower temperatures the polymer chains are relatively rigid and the free radicals formed by bond cleavages exist in a relatively well defined cage where recombinations or rearrangements are more likely. At higher temperatures, the polymer chains are more mobile and bond cleavages may result in chain displacement as well. The free radicals formed may be moved to an environment where further reaction is not energetically favorable.

Chapter Three

Experimental Methods

Sample Preparation

Prior to sample irradiation, Spectra-1000 fibers and fabric (Allied Signal Corporation, Petersberg, VA) were mounted in a rectangular aluminum frame and cleaned by soxhlet extraction in absolute ethanol (99.99%) for 24 hours. Though this procedure cleaned any physisorbed impurities or dirt loosely bound to the fiber surface, remnants of the commercially applied UV stabilizers and antioxidants were found by x-ray photoelectron spectroscopy. Soxhlet extraction in cyclohexane for 6 hours removed these additions. The cleaned fibers were then wrapped in acetone scrubbed aluminum foil and place in a dessicator at room temperature. Oxygen plasma- and corona- treated fibers processed by Allied Signal Corporation, Petersberg, VA, were cleaned and stored in the same manner.

Both fibers and fabric were prepared for ion irradiation by individually mounting approximately 100 fibers or several 100 mm x 0.5 mm fabric strips, with the use of double-sided sticky tape, on a 75 mm square aluminum frame. The frame was attached to a specially constructed aluminum fixture that kept the fibers and/or fabric in contact with a chilled curved aluminum heat sink as shown in Figure 3-1. The fixture also allowed the frames to be inverted so both sides of the fibers could be irradiated during separate runs.

High energy ion implantations were performed in a medium current implanter, with beam currents of approximately 20-30 μA, at the Spire Corporation, Danvers MA. Ion species, accelerating potentials, total ion doses and computed implant depths of the high energy ion implantations are shown in Table 3-1. The irradiation parameters were chosen so that a wide variety of ion masses would be represented. The ion energies were selected to correspond to approximately the same projected range. After irradiation the samples were kept in a dessicator.

Low energy Ar$^+$ ion irradiations were carried out with a 3-cm diameter Kaufman-type ion gun (Ion-Tech, Denver, CO), equipped with diverging beam optical grids,
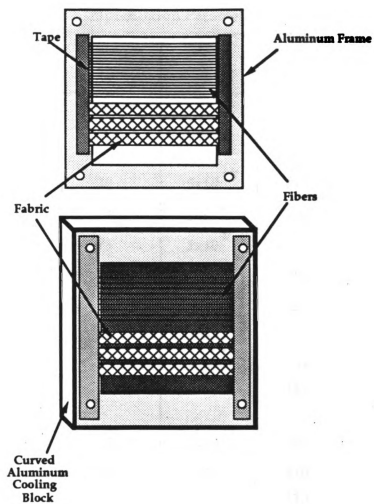
Figure 3-1: Fiber and fabric lay-up procedure.

Table 3-1: High energy ion implantation parameters.

High Energy Ion Implantation Parameters			
Ion Species	Energy keV	Dose ions/cm	Implant Depth, nm
Fibers:			
N^+	30	5×10^{14}	110
N^+	30	1×10^{15}	110
N^+	30	5×10^{15}	110
N^+	100	1×10^{15}	380
Ar^+	75	1×10^{14}	130
Ar^+	75	5×10^{14}	130
Ar^+	75	1×10^{15}	130
Ti^+	100	1×10^{15}	135
Na^+	40	1×10^{15}	110
Cl^+	80	1×10^{15}	145
Fabric:			
N^+	30	1×10^{15}	110
N^+	30	1×10^{14}	110
N^+	30	1×10^{13}	110
Ti^+	100	1×10^{15}	135
Xe^+	135	1×10^{15}	90

mounted inside an in-house cylindrical vacuum chamber (35 cm high and 20 cm diameter) pumped to a base pressure of 6.6×10^{-4} Pa as shown in Figure 3-2. The fibers were irradiated to doses ranging from 1×10^{15} to 1×10^{17} cm^{-2} at various accelerating potentials between 100 and 1000 eV. Ion current densities ranged from 0.130 to 0.341 mA/cm^2, as measured by a biased Faraday probe located on a shutter used to shield the fiber array prior to irradiation. The ion source to specimen distance was approximately 16.5 cm. Under these conditions, processing times ranged from 3.5 to 220 seconds. Processing parameters are listed in Tables 3-2 and 3-3.

Mechanical Tests

The tensile strength of both irradiated, plasma treated, corona treated and control Spectra 1000 fibers was measured using a United Testing Systems Model SFM-20 screw driven machine. The ends of individual fibers were attached to kevlar/epoxy composite grips (approximately 12 mm x 12 mm) with DER 331 epoxy cured with diethylenetriamine (DETA) using a 10/1 ratio. The adhesive was allowed to cure at room temperature for approximately 1 hour (until tacky). Binder clips were used to press the grips together for the remaining 24 hours. The 25 mm gage length coupons were tested at a crosshead speed of 2.54 mm/min. Prior to testing, an average fiber diameter was calculated from four diameter measurements made with an Olympus Micro Cue-300 video caliper. The tensile strength of the fiber was then calculated by using

$$s = F/A \qquad\qquad 3\text{-}1$$

where F is the load on the fiber at the failure and A is the fiber cross-sectional area.

Both treated and untreated fibers were composited with Epon 828 microdroplets so the fiber/matrix interfacial shear strength could be determined. Stoichiometric Epon 828 (diglycidyl ether of bisphenol-A, Shell Chemical Co.) with meta-phenelynediamine curing agent (m-PDA, 14.5 phr) epoxy microdroplets were deposited on individual fibers suspended across an aluminum frame by sliding a resin filled pipette along the length of the
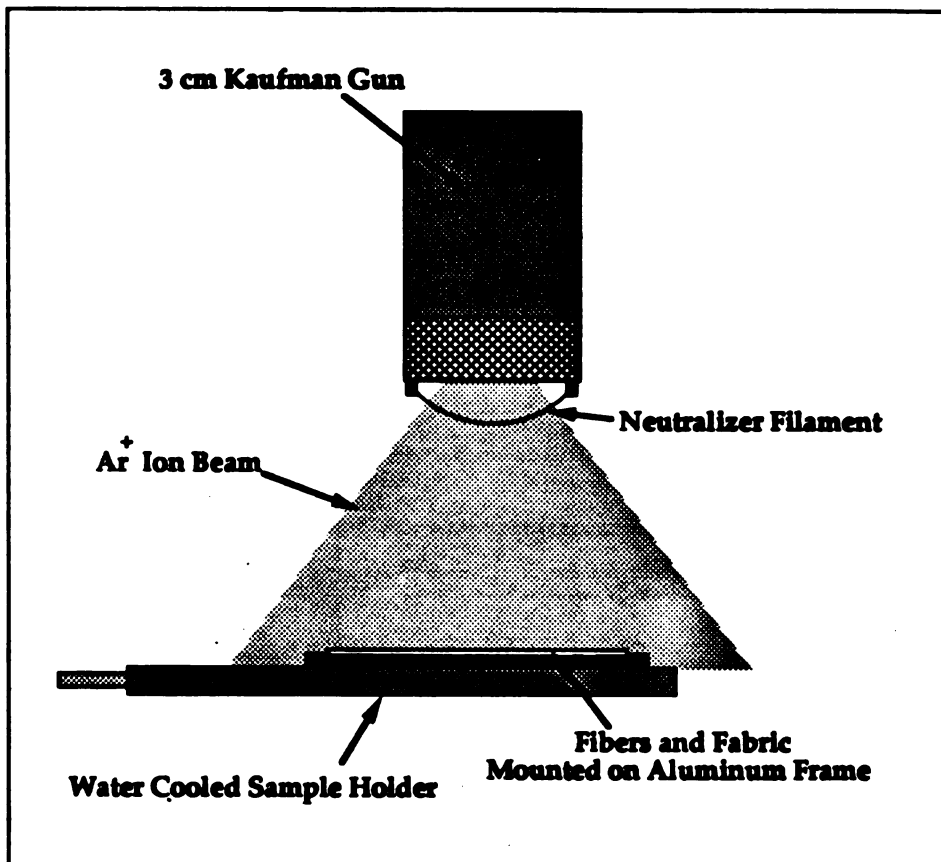
Figure 3-2: Illustration of low energy fiber irradiation arrangement.

Table 3-2: Low energy ion irradiation parameters, at a constant energy of 1 keV.

CURRENT DENSITY (mA/cm²)	PROCESSING TIME (sec)	DOSE x10¹⁵ (cm⁻²)	ION ENERGY (keV)	ION PROJECTED RANGE (nm)
0.260	1	1.6	1.0	5.5
0.158	3	3.0	1.0	5.5
0.146	5	4.6	1.0	5.5
0.354	3	6.6	1.0	5.5
0.246	5	7.7	1.0	5.5
0.341	5	10.0	1.0	5.5

Table 3-3: Low energy ion irradiation parameters, at a dose of 1×10^{16} cm^{-2}.

CURRENT DENSITY (mA/cm^2)	PROCESSING TIME (sec)	DOSE $\times 10^{16}$ (cm^{-2})	ION ENERGY (eV)	ION PROJECTED RANGE (nm)
0.124	22	1	100	1.4
0.217	10	1	250	2.5
0.316	3	1	500	3.5
0.267	7.5	1	750	4.3
0.341	5	1	1000	5.5

fiber. The microdroplets were cured with the fibers in a horizontal position at room temperature for 18 hours and then post cured for 2 hours at 348 K. This curing schedule ensured that no curing agent diffused out of the droplet during processing.

The microdroplet pull-out tests were performed using a blade micrometer attached to a microscope stage as shown in Figure 3-3. A composited fiber was glued to an aluminum plate using a cyanoacrylate adhesive which was attached to either a 50 or 250 gram load cell. The length of the droplet along the fiber axis, called the embedment length, was measured with the video caliper and recorded. A droplet was grasped by the micrometer blades and the micrometer moved away from the load cell at a rate of 20 microns/min. A 2 gram preload was applied to the droplet to facilitate fiber/tension axis alignment. The load vs displacement data was recorded either electronically or with a strip chart recorder. An average fiber/matrix interfacial shear strength, τ, was then calculated from

$$\tau = P_f / (\pi \bullet d \bullet l) \qquad\qquad 3\text{-}2$$

where P_f is the load at failure, d is the fiber diameter and l is the embedment length. The value of P_f, for each fiber treatment, was determined from the slope of a linear regression line constrained to pass through the origin of a plot of failure load versus embedment length for a number of 12 droplets as shown in Figure 3-4. Scatter in the data (for a given treatment) is believed to result from fiber surface heterogeneity [19], inherent weaknesses of the test itself (i.e., loading conditions and fiber free length [17]) and/or difficulty in the precise determination of the embedment area due to variable fiber radii. The ISS errors were determined by assuming a 95% confidence level. A minimum of 12 droplets were tested for each surface treatment.

The inherent irregular cross-sectional area of Spectra 1000 fibers makes an absolute determination of the fiber diameter extremely difficult. To minimize the uncertainty in the
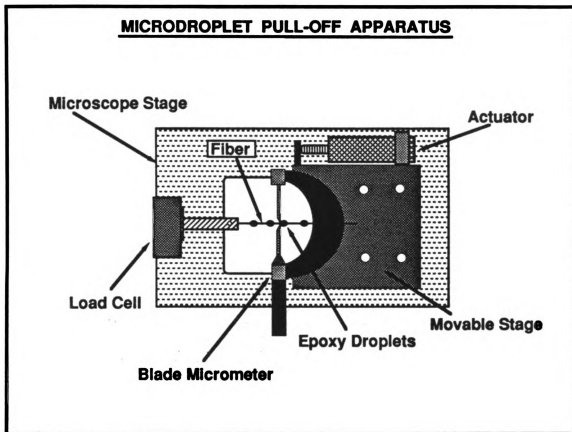
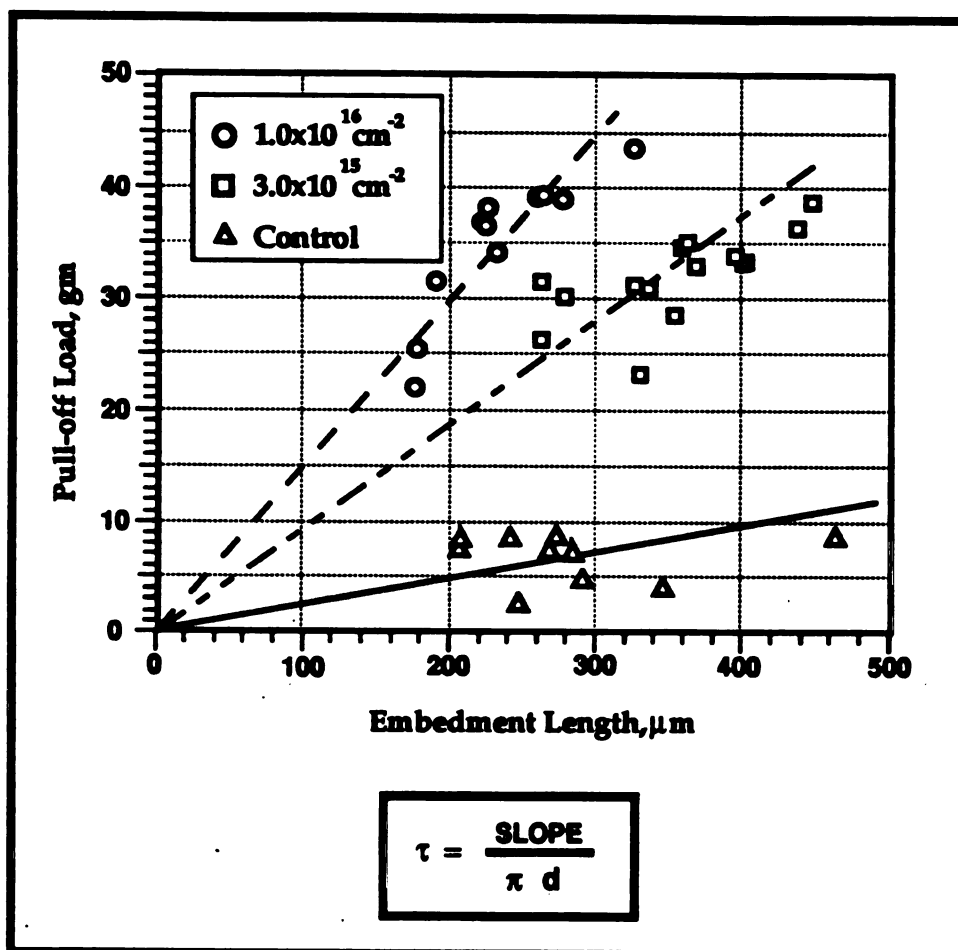Figure 3-3: Schematic diagram of the microdroplet pull-off apparatus.

Figure 3-4: Examples of pull-off load vs embedment length for 1 keV Ar⁺ ions.

ISS values due to the fiber diameter, ISS values were normalized with respect to the control value. ISS values cited were determined with a nominal fiber diameter of 30 μm.
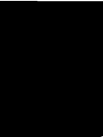
Surface Chemistry Characterization

X-ray photoelectron spectroscopy (XPS) spectra were obtained on a Perkin Elmer Phi 5400 ESCA system with a monochromatic Al Kα source (1486 eV) used to obtain both quantitative (relative surface concentrations) and qualitative (functional group) information within approximately the first 6 nm of the polyethylene fibers. The use of the monochromatic source precludes sample radiation damage. All samples used in this study were analyzed at ambient temperature and exhibited no evidence of x-ray damage during measurements. The pressure in the spectrometer was approximately 6.6×10^{-7} Pa. Five minute survey scans were taken for all treatments. A 15 minute multiplex scan on carbon (2-3 cycles) and oxygen (6-8 cycles) was performed for quantitative analysis. The implanted ion spectral peak was not observed.

Surface functional group chemistry characterization of the fiber surface was carried out on a Perkin Elmer 1850 Fourier Transform Infrared Spectrophotometer using an attenuated total reflectance (ATR-FTIR) technique. A KRS-5 (n = 2.38) internal reflecting element (IRE) with an angle of 45° was used to obtain the infrared spectra according to ASTM Annual Book 42, E573, 1984. Both treated and untreated fiber mats were purged of any adsorbed water by continuously flushing the fibers with dry air in a glove bag for a minimum of 1 hour. While in the glove bag, the mats (approximately 12mm x 40mm) were mounted on both sides of the crystal so that the beam underwent approximately 25 reflections, with a penetration depth of 2 to 3 μm before striking a mercury cadmium telluride detector (Figure 3-5). The sample holder was then placed in the sample chamber which was subsequently purged with dry air for either 15 or 30 minutes.

Spectra were scanned 1000 times (approx. 6 min.) and stored in memory. Background spectra of the IRE only were taken with the same exact purging and scanning

conditions prior and subsequent to spectra of fiber mats. The background spectrum was then subtracted from the fiber mat spectrum resulting in the final spectra.

Physico-Chemical Characterization

Surface energy was measured via static advancing contact angles for single fibers using a micro-Wilhelmy technique. Water, methylene iodide and ethylene glycol were used as characterizing liquids, as shown in Table 3-4. Fibers, 15 mm in length, were attached with cyanoacrylate adhesive to a nickel hook which was hung on a Cahn Rg electrobalance. The electrobalance measured the force on the fiber as it was raised and lowered in the characterizing liquid (Figure 3-5). Approximately 3 mm of the fiber was immersed before being moved in and out of the liquid at a rate of 25 μm/s. The fibers were allowed to stabilize 20 seconds before the static force measurement was taken. The entire apparatus was enclosed in an environmentally controlled chamber to eliminate wind currents, reduce contamination of the characterizing liquid, insulate the apparatus from vibrations and maintain constant temperature.

Contact angles were determined (neglecting buoyant force) according to

$$m \cdot g = \gamma_{l,t} \cdot P\cos\phi \qquad\qquad 3\text{--}3$$

where m is the mass measured by the electrobalance, g is the acceleration due to gravity, P is the perimeter of the fiber and $\gamma_{l,t}$ is the total surface energy of the probe liquid. The average fiber diameter, 31.2 +/- 2.8 μm, was determined by assuming complete wetting (ϕ = 0) using hexadecane as a characterizing liquid. A minimum of 45 measurements were taken for each fiber treatment.

Surface energetic analyses of the fiber were determined from the equilibrium advancing contact angles in the manner described by Kaeble, et al. [56]. This method assumes, for low surface energy solids such as polymers, that the total surface free energy across the interface, $\gamma_{i,T}$, is composed of a polar, $\gamma_{i,P}$, and a dispersive part, $\gamma_{i,D}$:
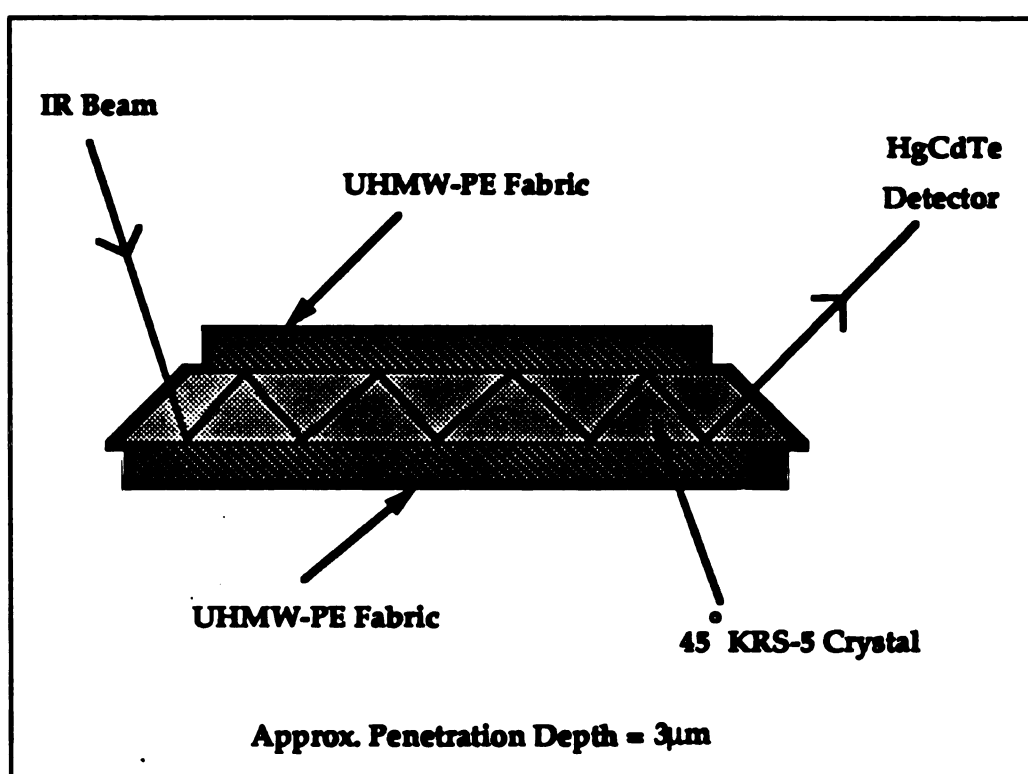
Figure 3-5: Schematic diagram of attenuated total internal reflectance technique.

Table 3-4: Surface energies of characterizing liquids for the micro-Wilhelmy experiments.

Table 3-4			
Surface Energies of Characterizing Liquids, mJ/m^2			
Liquids	$\gamma_{L,t}$	$\gamma_{L,d}$	$\gamma_{L,p}$
Water	72.8	21.8	51.8
Ethylene Glycol	48.3	29.3	19.0
Methylene Iodide	50.8	48.4	2.4
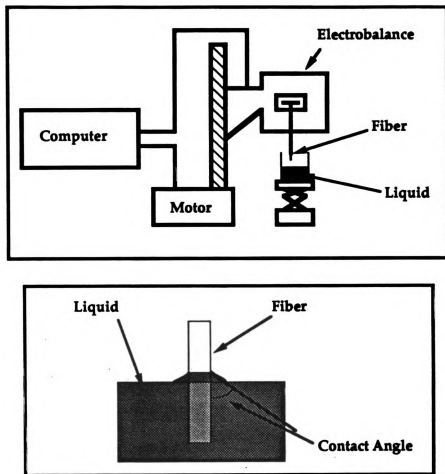
Figure 3-6: Schematic diagram of the micro-Wilhelmy apparatus.

$$\gamma_{i,T} = \gamma_{i,P} + \gamma_{i,D} \qquad\qquad 3\text{-}4$$

where i stands for either the fiber or liquid. The work of adhesion is given by:

$$W_a = 2[\ \gamma_{F,D}^{1/2}\gamma_{L,D}^{1/2} + \gamma_{F,P}^{1/2}\gamma_{L,P}^{1/2}] \qquad\qquad 3\text{-}5$$

or in terms of the contact angle as

$$W_a = \gamma_{L,T}[\ 1 + \cos\phi\ ]. \qquad\qquad 3\text{-}6$$

This leads to:

$$W_a/2\ \gamma_{L,D}^{1/2} = \gamma_{F,D}^{1/2} + \gamma_{F,P}^{1/2}[\gamma_{L,P}^{1/2}/\gamma_{L,D}^{1/2}] \qquad\qquad 3\text{-}7$$

which is expressed in a slope-intercept form. Measuring the contact angle for a minimum of two liquids and plotting $W_a/2\ \gamma_{L,D}^{1/2}$ vs $\gamma_{L,P}^{1/2}/\gamma_{L,D}^{1/2}$ yields a straight line with slope and intercept equal to $\gamma_{F,P}^{1/2}$ and $\gamma_{F,D}^{1/2}$ respectively.

Samples of irradiated fabric for gel-fraction determination were placed in acetone washed 200 mesh stainless steel gauze. Extraction of the sol-fraction was performed by suspending the gauze in boiling p-xylene, containing 0.5 wt.% of anti-oxidant (2,6-di-t-butyl-4-methylcresol) for 24 h. The samples were then repeatedly dipped in fresh boiling xylene until no polymer remants remained. The samples were deswollen in acetone and dried under vacuum at 223 K for 6 h. The gel-fractions were determined by the weight difference of the sample before and after extraction.

Microscopy

A Hitachi S-2500 scanning electron microscope (SEM), equipped with a LaB$_6$ filament operating at 10 or 15 kV, was used to obtain micrographs of the fiber and fracture surfaces. For surface investigation, fibers 10 mm long were mounted on a piece of double-sided sticky tape, placed on a screw and sputter coated with approximately 20 nm of Au to provide a conductive link to the SEM. The screw was installed on a high resolution stub which could be rigidly locked to the objective polepiece to minimize image degradation due to vibration. Under these conditions, beam damage began to degrade the fibers after only
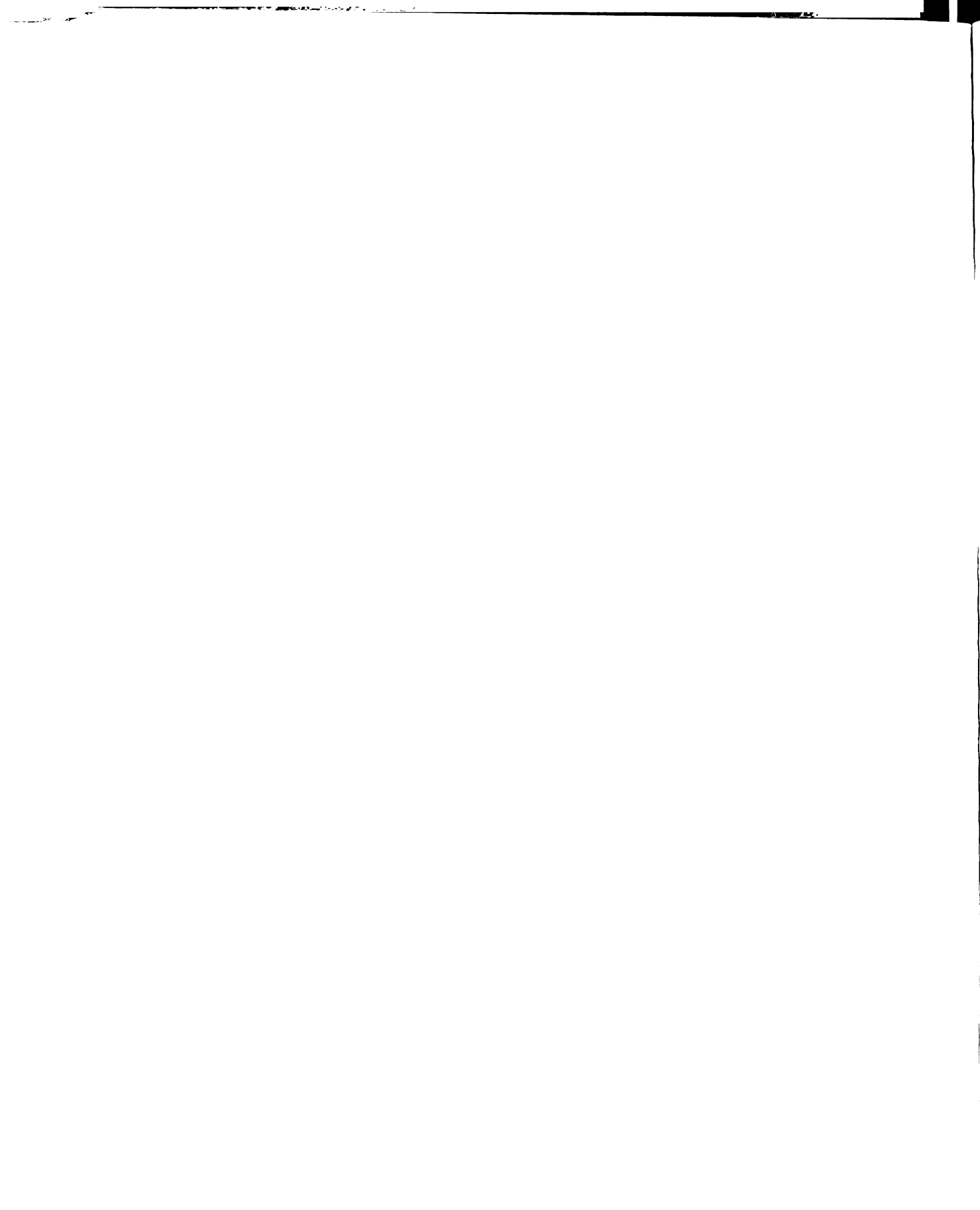
30-60 seconds of exposure at high magnification. Thus, after focusing and stigmation were completed, the specimen was translated slightly, and the micrograph recorded from an undamaged section of the fiber surface. Resolution under these circumstances was approximately 10 nm point to point.

Specimens of tested and untested microdroplets were attached to copper tape and sputter coated with approximately 20 nm of Au. The specimens were turned over and the other side coated with Au also. The taped specimens were then placed on a graphite holder and mounted in the SEM for viewing.

Transmission electron microscopy (TEM) of the fiber-matrix interface was accomplished by imaging room temperature ultra-thin microtomed sections of single fibers embedded in Epon 828 epoxy matrix as described in reference 57. The specimens were imaged in a JEOL 100 CX TEM at an accelerating voltage of 100 kV.

Chapter Four

RESULTS and DISCUSSION

This chapter is divided into two main sections corresponding to the two different

implantation energy regimes studied: high energy (> 30 keV) irradiations performed in a

medium current ion implanter, and low energy ion irradiations performed by a 3 cm

diameter ion Kaufman type ion gun. The high energy implantation experiments, which are

a continuation of an earlier study, will be discussed first.

High Energy Ion Implantation of Spectra -1000

Visual Observations   The most obvious effect of high energy ion implantation on Spectra

is the surface discoloration as shown in Figures 4-1a and 4-1b. The color change of the

fabric irradiated with 30 keV N^+ ions as a function of dose is illustrated in Figure 4-1a. No

color change occurs for either the 1×10^{13} or 1×10^{14} cm^{-2} irradiations (low dose regime),

while the 1×10^{15} and 1×10^{16} cm^{-2} (high dose regime) samples appear gold and dark

brown, respectively. In the high dose regime the darkening occurs because preferential

sputtering depletes the number of fiber surface hydrogen atoms leaving large amounts of

saturated carbon bonds in a graphite-like structure [58].

Figure 4-1b illustrates the color differences for irradiations with different ion

species (Xe^+, Ti^+, N^+, N^+) and different ion energies (135 keV, 100 keV, 30 keV and 1

keV respectively) at a constant dose of 1×10^{15} cm^{-2}. Comparison of the 1 keV and 30 keV

N^+, 1×10^{15} cm^{-2} implanted samples indicates a difference in color intensity. The

difference occurs because the higher energy ion produces more damage (molecular

excitations and ionizations, combined with atomic displacements) altering the optical

properties of the material more extensively. The different ion masses and energies for the

other irradiated samples make direct comparisons invalid, but the more massive and
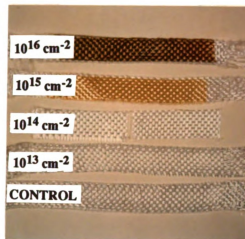
(a)
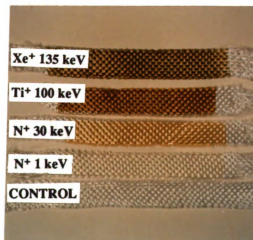
(b)

Figure 4-1: Photographs showing the discoloration of Spectra-1000 irradiated..
as a function of (a) dose and (b) ion

energetic Xe^+ and Ti^+ implantations produce more radiation damage, resulting in a higher level of carbonization.

Surface Chemistry   An ATR-FTIR investigation on irradiated UHMW-PE (in fabric form) revealed a oxidized fiber surface . The evolution of the surface functional groups for 30 keV N^+ irradiated fabric, as a function of dose, is illustrated by the IR spectra in Figure 4-2. The probe depth of ATR-FTIR is 2 to 3 μm, much deeper than the predicted depth of irradiation induced surface modification (approximately 135 nm). The data thus represent both irradiated and unirradiated material characteristics. The control spectra shows characteristic absorbances at 2925 cm^{-1} (CH stretch) and 1420 cm^{-1} (CH$_2$ scissors and in-plane bending), seen also in the irradiated spectra. All spectra exhibit a slight non-linear baseline due to the large number of scattering centers in the fabric. The absorbance peaks below 1400 cm^{-1} are due to the rubber pressure pads making intimate contact with the reflecting crystal through the holes in the fabric.

Comparison of the control (unirradiated) and 1×10^{13} N^+ cm^{-2} dose spectra in Figure 4-2 shows the appearance of absorbance bands at wavenumbers identified by the letters A, B and C. The presence of these peaks at such low doses indicates the sensitivity of polymers to ion beam irradiation when compared to ceramics or metals (where few effects are seen at doses less than 1×10^{15} cm^{-2}). The assignment of the functional groups to these absorbance bands are made according to Gedde and Ifwarson [59] and Schaible, et al. [55]. In Figure 4-2, the peak indicated by A, at 1644 cm^{-1}, has not been conclusively identified, but may be bicyclic quinone systems, which absorb in the region between 1635 and 1655 cm^{-1}. The peak at B (1704 cm^{-1}) is due to carbonyl groups (C=O). At point C is a broad band representing both hydroxyl (OH) and hydroperoxide (OOH) groups.

As the ion dose increases, small absorption structures develop into strong, broad composite absorbance bands, indicated by letters C and D. These bands represent extensive surface oxidation at the highest dose of 1×10^{16} N^+/cm^2. The carbonyl stretching
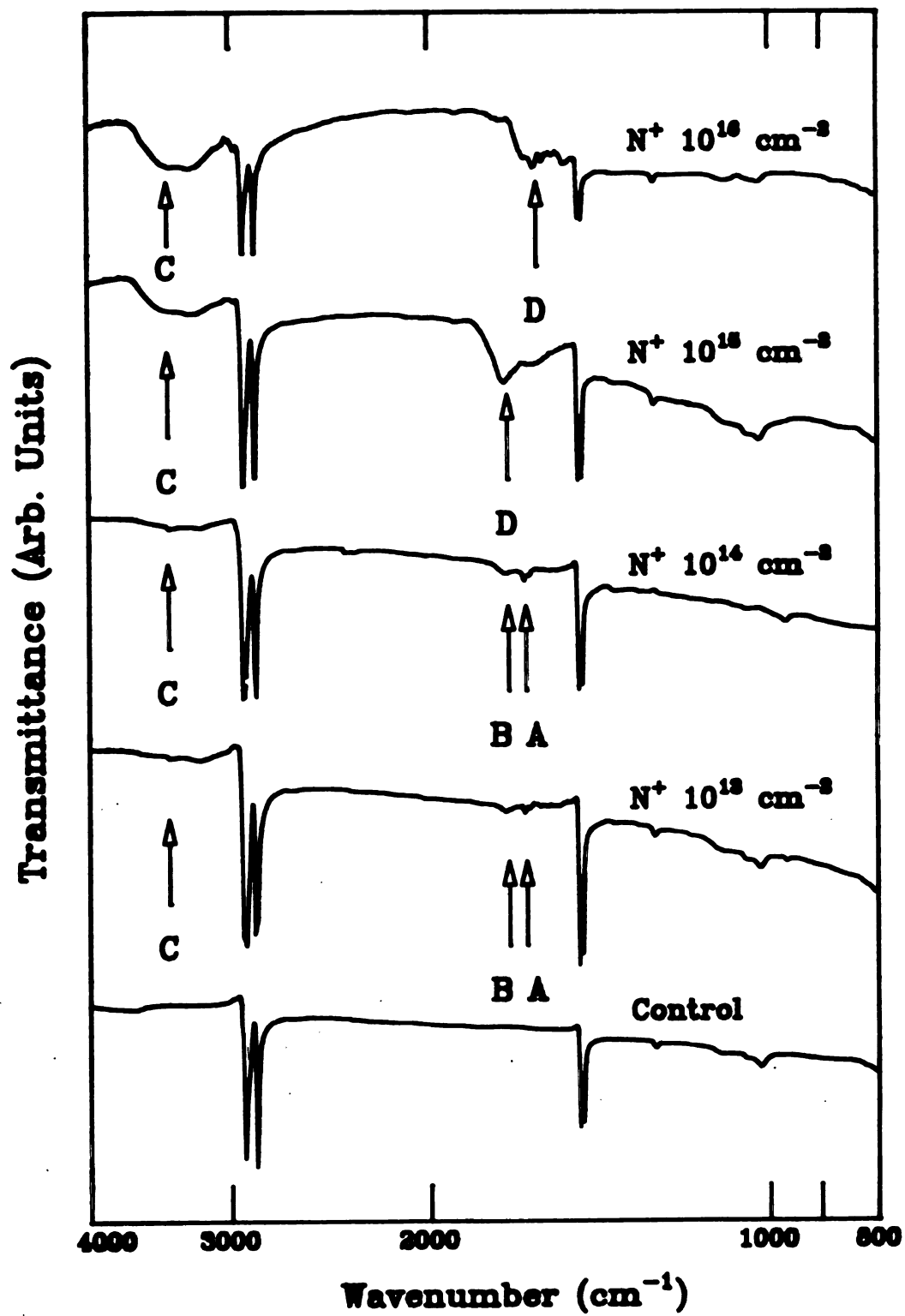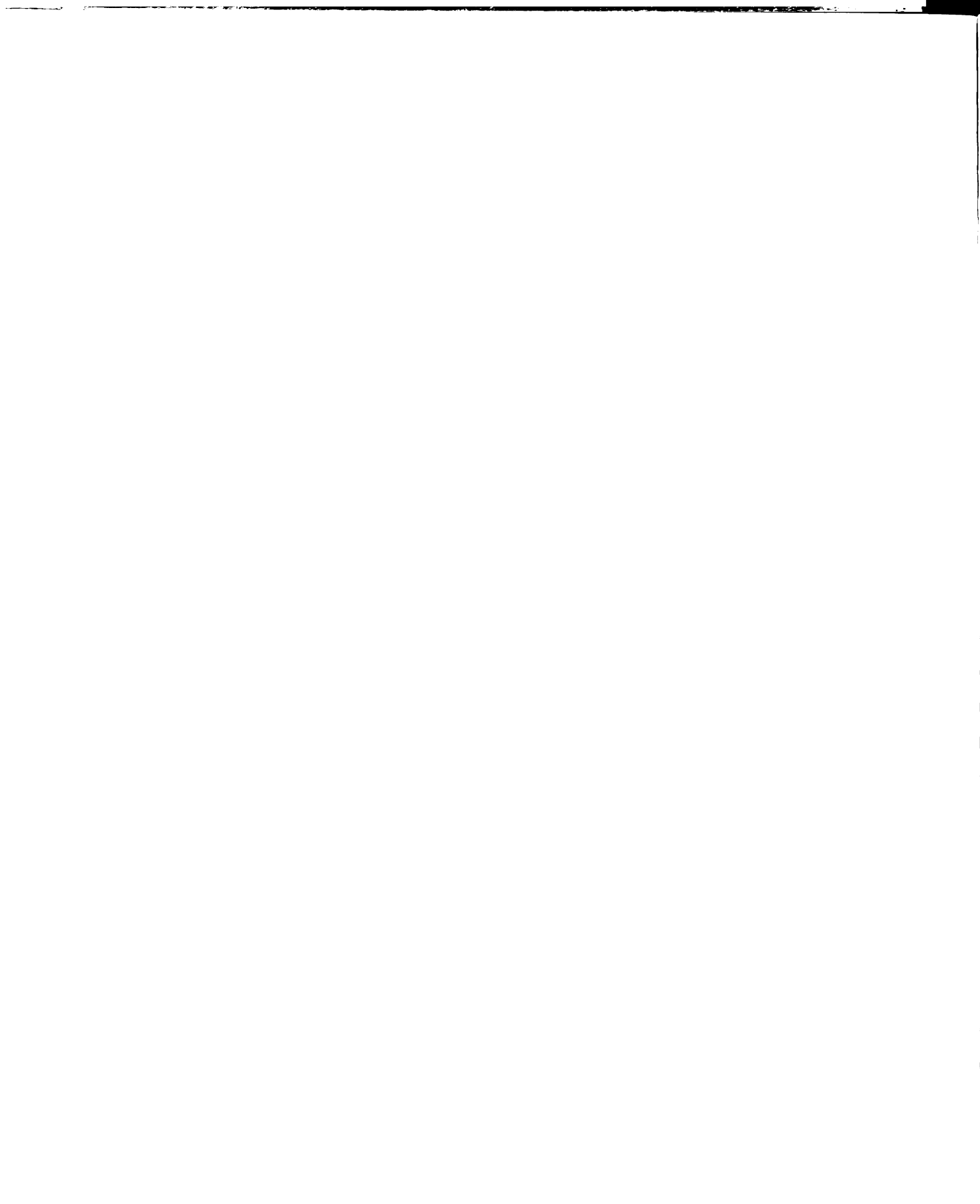
Figure 4-2: ATR-FTIR spectra for various doses of N^+ ion implantation.

band, A, consists of three overlapping components which may be assigned to saturated aldehydes (1733 cm^{-1}), saturated ketones (1721 cm^{-1}), saturated acids (1712 cm^{-1}) and possibly unsaturated hydrocarbons [60]. The poor specificity of these carbonyl groups is inescapable because the separations between the peak positions are comparable to, or less than, the half-widths of the three peaks, and appreciably greater than the spectrometer resolution (4 cm^{-1}). The permanent dipole moments of these surface groups produces a polar molecules. At a dose of 1×10^{16} N$^+$/cm^2 the large absorbance band at D changes shape possibly due structural modifications such as formation of a crosslinking network, severe hydrogen depletion and increases in aromatic ring structures, brought about by the overall degradation of the polymer.

These results agree qualitatively with those of Ishitani, et al. [54] who studied 60 keV oxygen implanted polyethylene and reported a maximum surface oxidation level (measured by ATR-FTIR) at a dose of 5×10^{14} cm^{-2}. They also observed that, as the dose was increased above 5×10^{14} cm^{-2}, most absorbance peaks decreased, except for an increase in the concentration of unsaturated hydrocarbons.

Figure 4-3 shows the IR spectra for three different ion species (nitrogen, titanium and xenon) with differing energies at a constant dose of 1×10^{15} cm^{-2}. In general, the structure of the bands at points A and B in these spectra are similar. The absorbance band at point A in the Xe$^+$ and Ti$^+$ implantations appear closer in structure to 1×10^{16} N$^+$/cm^2 irradiations than the 1×10^{15} N$^+$/cm^2 samples. Since the Xe$^+$ and Ti$^+$ masses and ion energy are greater than N$^+$ ions, less radiation damage occurs during the N$^+$ irradiations resulting in slight surface oxidation differences. With this qualification, the degree and type of surface oxidation is relatively independent of ion species. A plausible explanation for this insensitivity can be made by considering the fundamental aspects of the ion-polymer interactions. Upon irradiation, the ions lose energy by ionizing and exciting molecules, creating both unstable free radicals (which recombine rapidly), and more stable radical species. (The term free radical refers to any non-saturated fragment and does not
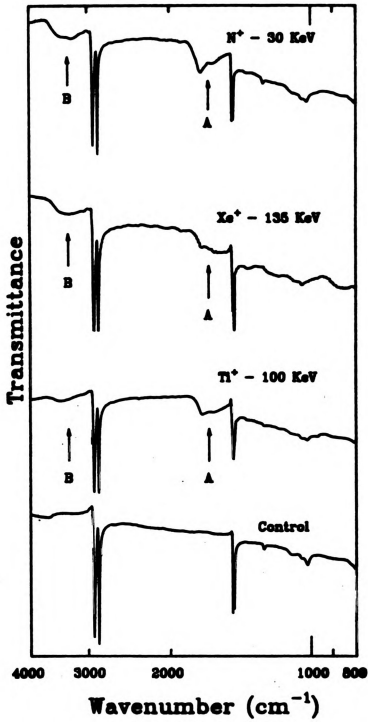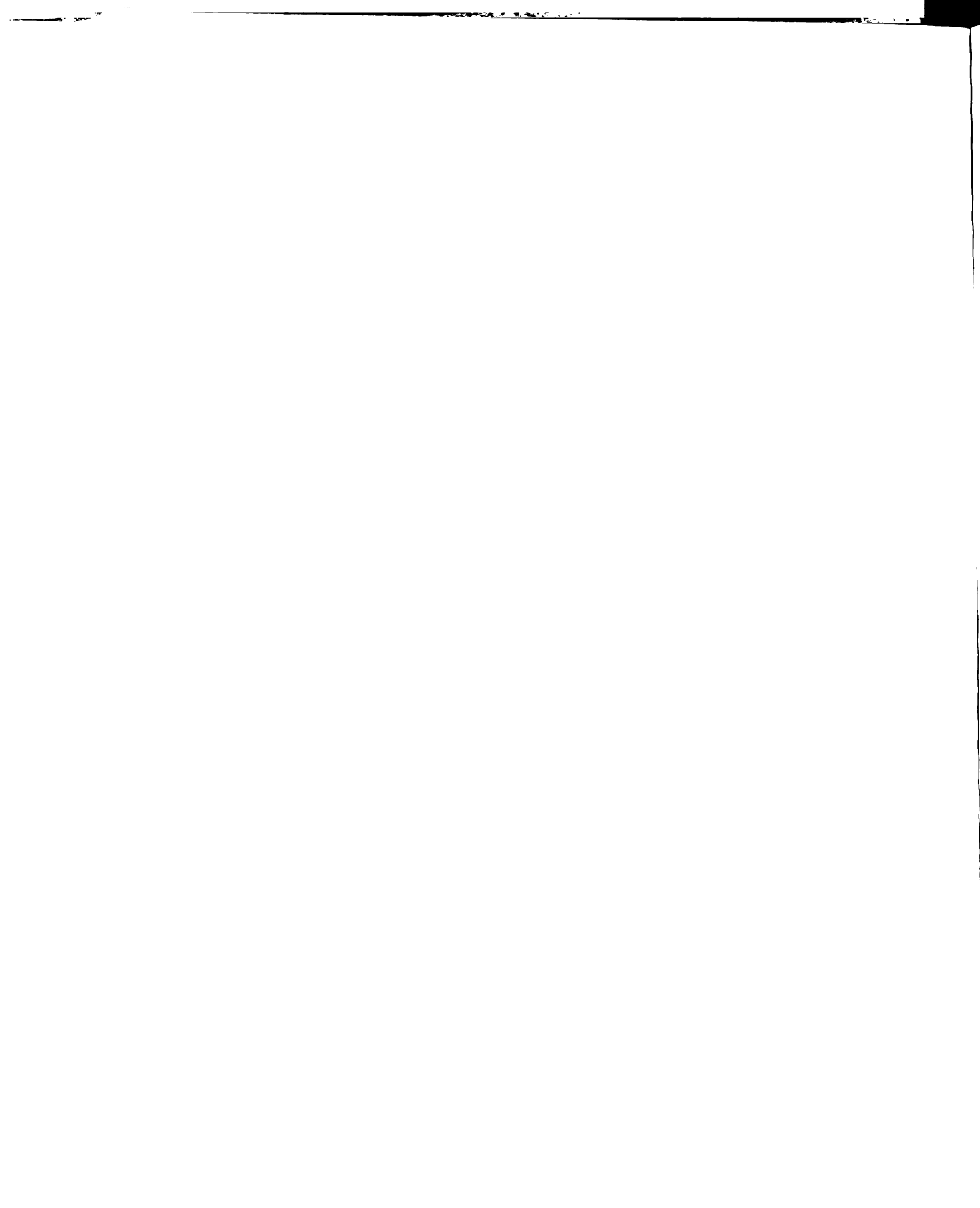
Figure 4-3:   ATR-FTIR spectra for N^+, Ti^+ and Xe^+ ions at 1×10^{15} cm^{-2}.

necessarily refer to spatial freedom of the ionized specie.) Species insensitivity has been documented by Chipara and Georgrscu [61], who determined that the nature of the radicals in irradiated polymers depends mainly on the energy deposited by the incident particle rather than on the type of incident particle. Thus, the surface oxidation of ion irradiated Spectra-1000 relies on the free radical generation and not the exact details of what initiated the production of these free radicals.

The source of oxygen has not been conclusively determined, though at processing pressures of 5×10^{-6} Torr, low but finite oxygen partial pressures existed in the vacuum chamber during implantation, making oxygen addition surface reactions possible. A calculation of the impingement rate, R, of O_2 molecules on the fiber surface during irradiation follows from

$$R = p(2\pi MWkT)^{-0.5} \qquad\qquad 4-1$$

where p is the oxygen partial pressure, MW the molecular weight of the gas, k is Boltzmann's constant and T the temperature [62]. For an oxygen partial pressure of 1×10^{-7} Pa at a temperature of 300 K the impingement rate is 2.7×10^{11} atoms cm^{-2} s^{-1}. Since the areal density of most solids is 5×10^{14} to 3×10^{15} atoms cm^{-2} complete oxidation of the fiber surface is not likely to occur before the irradiation chamber is bled to atmosphere. Additional oxidation reactions then proceed from post-irradiation exposure to atmospheric oxygen.

Further surface chemical analysis was performed using x-ray photoelectron spectroscopy (XPS). Survey scans of UHMW-PE control fabric and 30 keV, 1×10^{15} N^+/cm^2, irradiated fabric are shown in Figure 4-4 and Figure 4-5. The spectra show an intense peak centered at 284.6 eV, due to the carbon 1s core level electrons (C1s) and one centered at 532.0 eV for the oxygen 1s core level electrons (O1s). The oxygen KLL Auger peaks at 977.0 and 998.0 eV are also observed in these spectrum. Presumably the oxygen present in the control spectra is due to processing or commercially applied antioxidants and
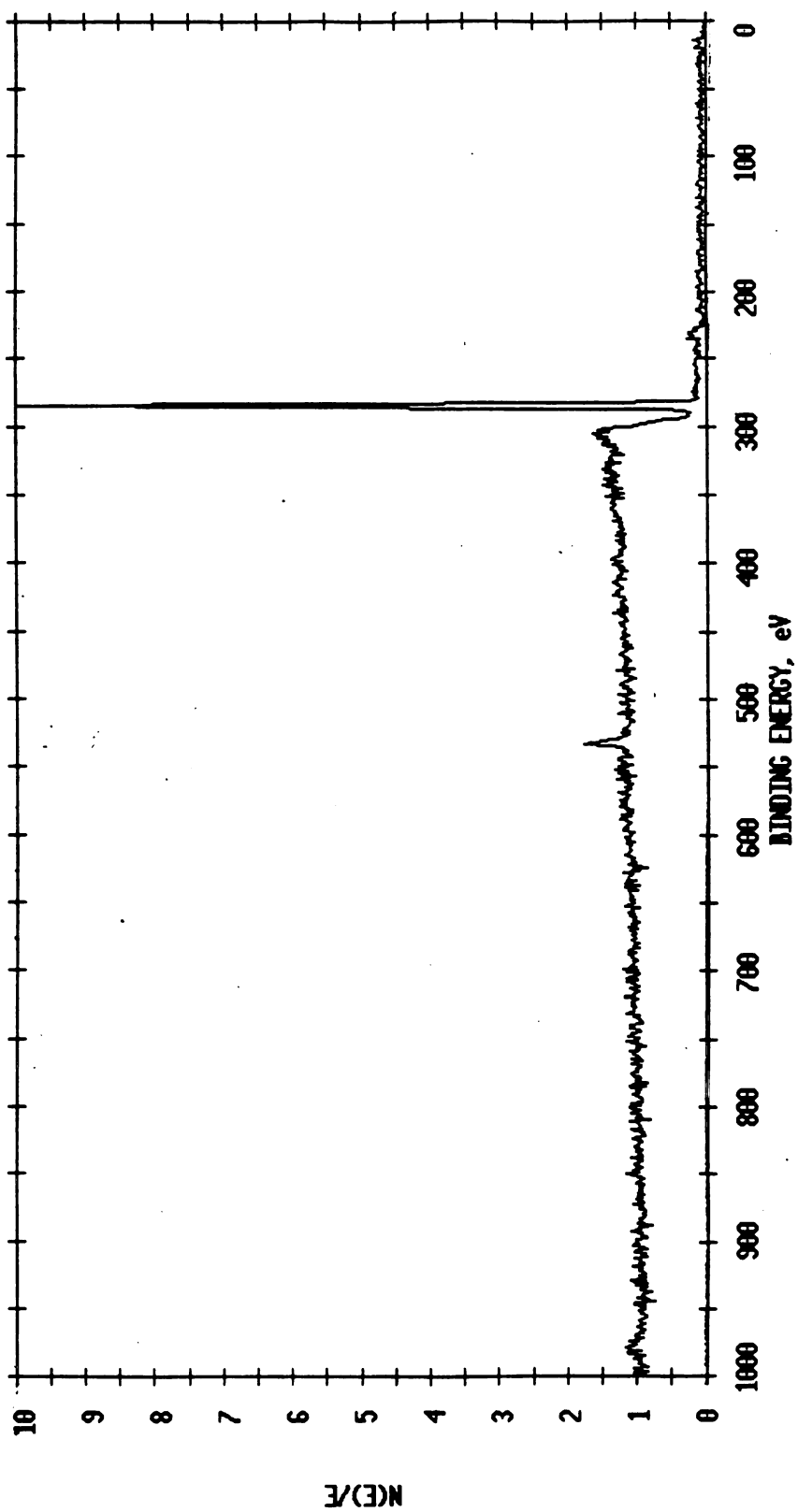
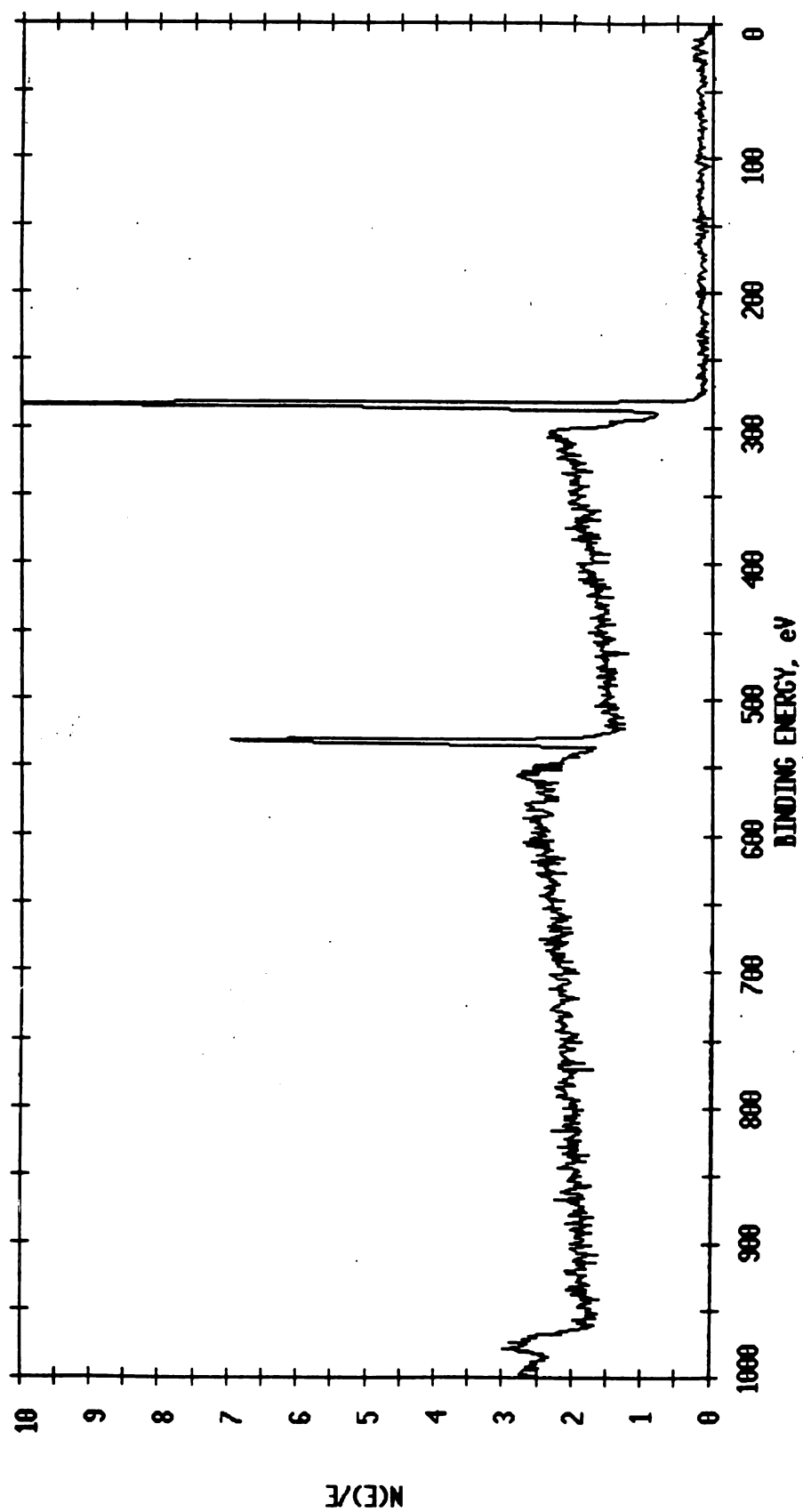Figure 4-4: A typical survey scan of untreated Spectra-1000 fabric.

Figure 4-5: A typical survey scan of Spectra-1000 fabric irradiated by 30 keV N^+ ions irradiated to a dose of 1×10^{15} cm^{-2}.

UV stabilizers not removed by the ethanol wash. No presence of the implant species was found in the survey scan of the irradiated samples.

High resolution scans of the C1s region for control and fabric implanted by 30 keV N^+ to a dose of $1x10^{15}$ cm^{-2}, shown in Figure 4-6 and Figure 4-7, were undertaken to further investigate the type chemical bonding occurring on the fiber surface. The control C1s peak is relatively narrow (~1.75 eV FWHM) centered at 285.0 eV, but slightly broader than that expected for pristine polyethylene, possibly due to small amounts of oxygen-carbon bonding. The C1s peak for the N^+ implanted specimen is asymmetric and broader toward the higher binding energies, providing evidence for higher oxidation states of carbon such as alcohol/ether (286.1 eV), peroxide (286.6 eV), carbonyl (287.6 eV) and ester/carboxyl groups (290.0 eV). Line-shape analysis, using a deconvolution routine, was performed on the high resolution scans to more exactly determine the chemical state of the oxidation, but no reasonable fits were obtained.

The relatively narrow width of the C1s peak indicates that the irradiation altered the surface chemistry, but not sufficiently to produce significant amounts of C-O type bonds at the higher binding energies. These results correlate well with those results reported by Lanauze and Myers [63] for corona treated polyethylene. Other corona discharge treatment studies [64] indicate large numbers of carbon-oxygen functionalities. Furthermore, our results are also quite different from those obtained by an XPS study for argon, nitrogen and oxygen plasma treated polyethylene, where extremely broad C1s peaks revealed the highly oxidized nature of the surface [65]. Thus the degree and type of surface oxidation varies widely for different processing techniques and processing parameters.

Figure 4-8 shows the oxygen:carbon composition ratio of UHMW-PE fabric irradiated by 30 keV N^+ ions as a function of ion dose, determined by XPS. The surface oxygen concentration increases significantly from the control value of 3.5 at.% to a maximum value of 16.5 at.% for an ion dose of $1x10^{15}$ cm^{-2} then decreasing 11.2 at.% for the highest dose of $1x10^{16}$ cm^{-2}. Schaible, et al. [55] has reported that an equilibrium free
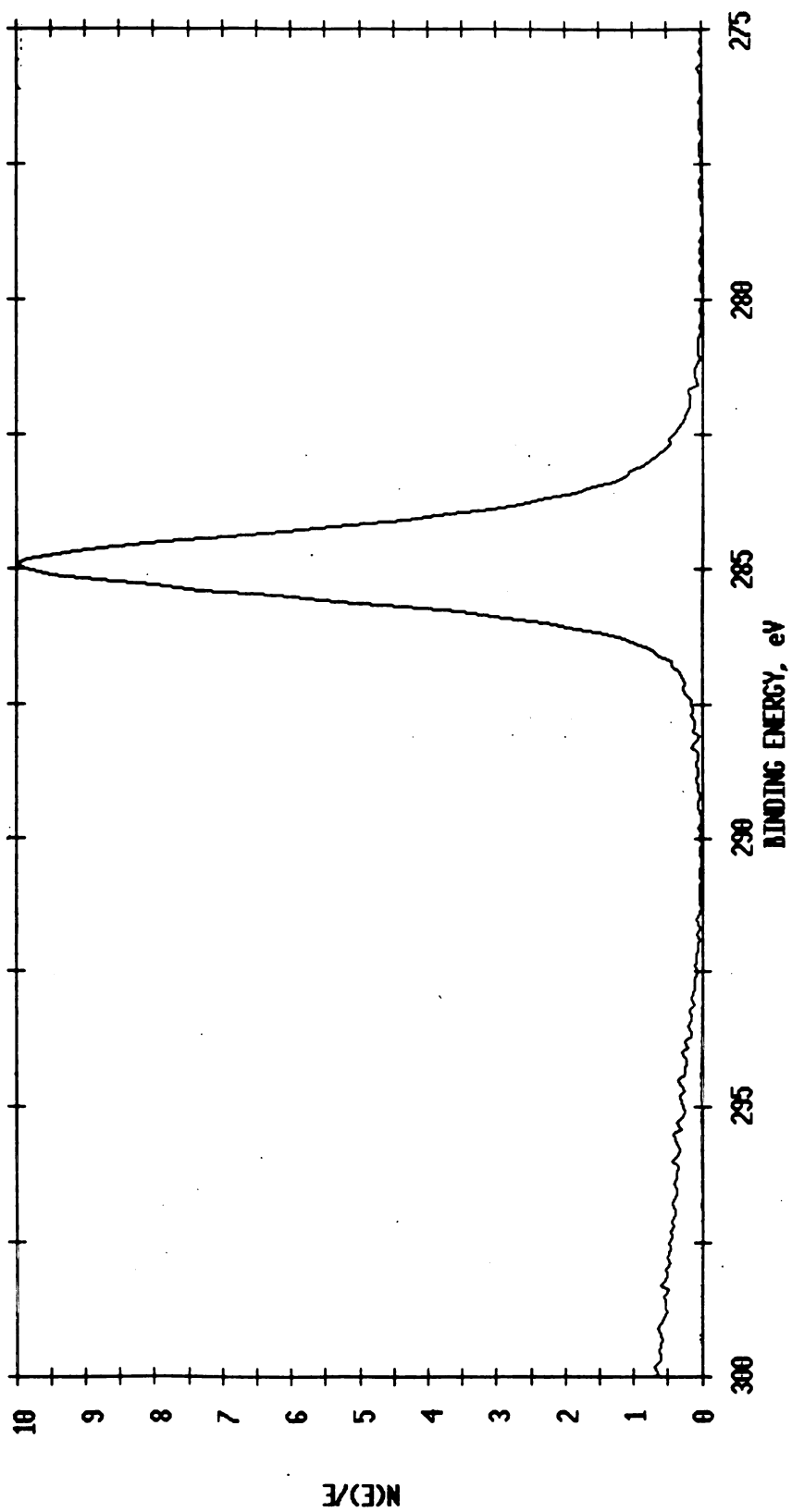
Figure 4-6: A high resolution scan of the C1s region for untreated Spectra-1000 fabric.
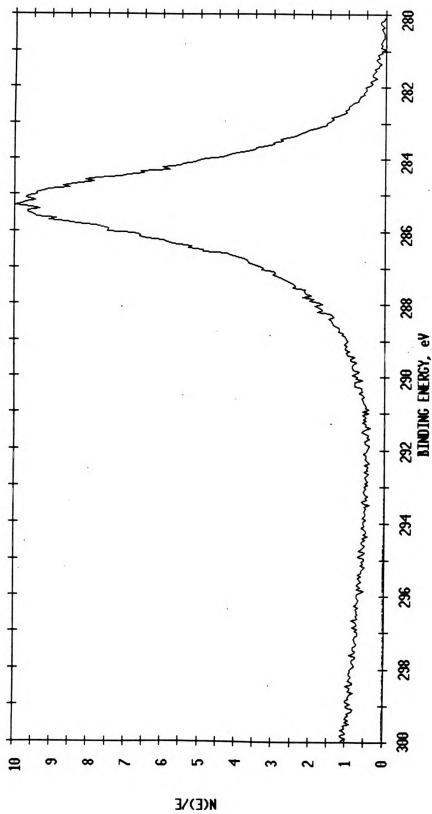
Figure 4-7: A high resolution scan of the C1s region for Spectra-1000 fabric irradiated by 30 kev N⁺ ions to a dose of 1x10¹⁵ cm⁻².
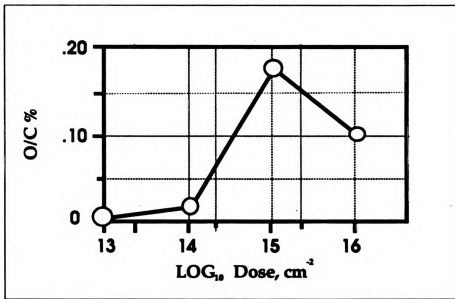
Figure 4-8: Oxygen:carbon ratios as a function of ion dose for UHMW-PE fabric irradiated by 30 keV N$^+$ ions.

radical concentration (the value of which depends on the specific irradiation conditions) plateaus at doses above approximately 3×10^{15} cm^{-2}, independent of ion type and energy. The increased concentration of unsaturated aromatic structures, at least partially, is responsible for the decrease in oxygen containing groups.

SEM Observations   The degree of mechanical interlocking between the fiber and matrix is another important factor in the development of good interfacial bonding. Interlocking tends to increase as the surface morphology of the fiber becomes rougher. Figures 4-9 and Figure 4-10 show a rather striking comparison between the surface morphology of Spectra-1000 fibers in the untreated, ion beam modified, plasma and corona treated conditions (the two latter representing commercially processed fibers supplied by Allied-Signal Corp., Petersburg, VA).

Untreated fibers, shown in Figure 4-9a, have a relatively smooth surface in the axial direction of the fiber, with numerous loosely bound tendrils curling up from the surface. After a 30 keV N$^+$ irradiation to a dose of 1×10^{15} cm^{-2}, as shown in Figure 4-9b, the tendrils have been removed, or else welded down to the fiber surface, but the surface remains smooth. The welding effect probably results from thermal effects of the beam, which may cause greater local heating in the tendrils due to their larger thermal separation from the heat sink. The effect would be magnified by the low thermal conductivity (0.15 to 0.67 W m^{-1} K^{-1}) and low melting point of polyethylene, and the lack of a convective heat transfer route in the vacuum of the implantation chamber.

The untreated fiber and the ion beam modified fibers have surface morphologies which are in sharp contrast to the plasma and corona treated fibers shown in Figures 4-10a and 4-10b, respectively. Here the fiber surfaces are extremely rough, with numerous slit-like cavities in the transverse direction; however, the slit-like cavities are not uniformly distributed. This type of surface morphology should provide enhanced mechanical interlocking (assuming that good wetting can be achieved), but the cavities
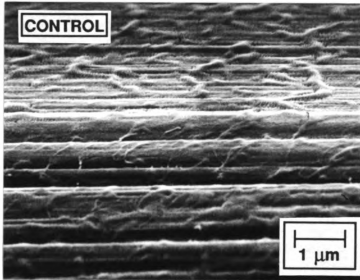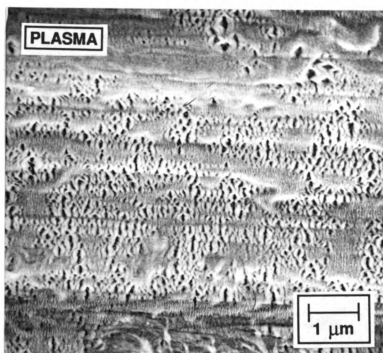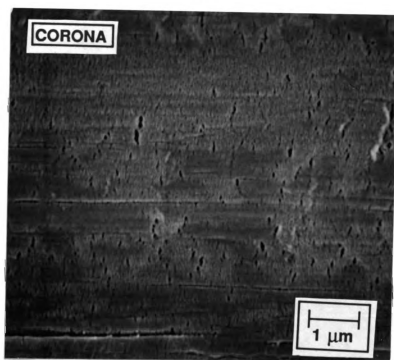
(a)
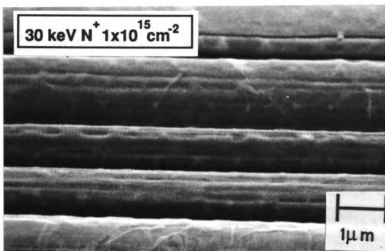
(b)

Figure 4-9: SEM micrographs of (a) control and (b) ion irradiated (1×10^{15} N+/cm^2) treated fibers.
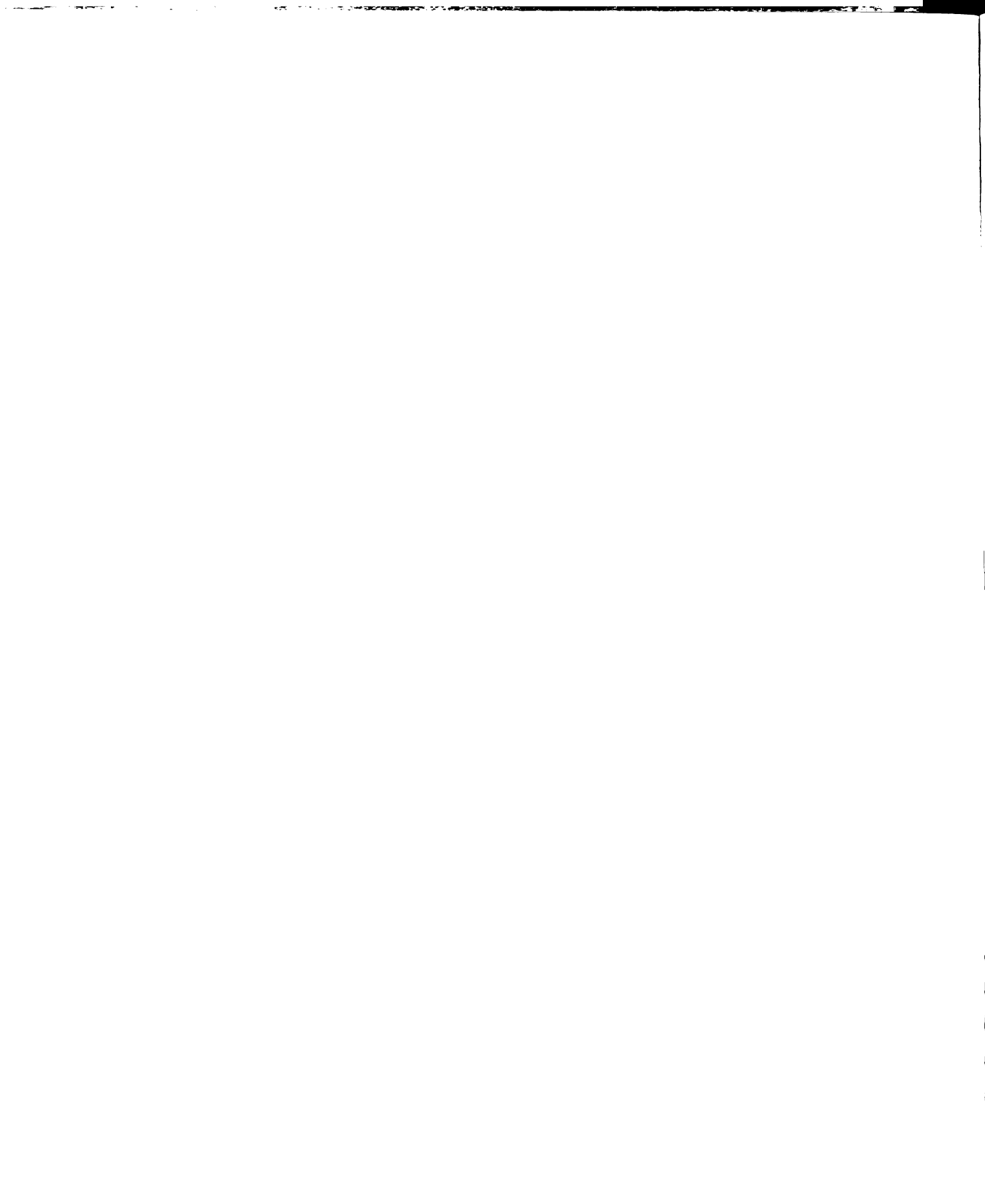
(a)

(b)

Figure 4-10: SEM micrographs of (a) plasma treated and (b) corona treated fibers.

can act as stress concentrating flaws, weakening the plasma treated fiber in tension. A reduction of 12% of the control tensile strength was measured. (The tensile strength of the corona treated fiber was not tested.) Microdroplet pull-off tests indicated 200% and 300% increases in the interfacial shear strength of plasma and corona treated fibers over that of untreated fibers.

Our results indicate that high energy irradiations only slightly altered the fiber surface morphology, while the plasma and corona treatments radically modified the surface morphology. The pitted fiber surface produced by the plasma and corona treatments will increase the amount of mechanical interlocking resulting in better adhesion. Changes produced by high energy irradiations may not actually increase mechanical interlocking; however, by removing and welding loosely bound tendrils and on the fiber surface and inducing crosslinking in the implanted region, the cohesive strength of the fiber surface will increase, resulting in increased ISS as reported by Ozzello et al [8]. Moreover, the sputtering that occurred during irradiation would tend to remove any low molecular weight species and weak boundary layers present on the fiber surface, improving the chances for increased adhesion.

TEM Observations   Ultra-thin sections of control and ion irradiated Spectra-1000 fibers, microtomed transverse to the fiber axial direction for imaging in a transmission electron microscope, help document the locus and mode of fiber-matrix interfacial failure. A large number of transverse untreated UHMW-PE fiber-matrix sections were examined, with fiber dropout from the matrix (the most commonly observed feature) suggesting extremely poor fiber-matrix adhesion. A typical example where the fiber remained in the matrix is shown in Figure 4-11a. A higher magnification view of the fiber-matrix interface in Figure 4-11b shows that decohesion results in fibrillated structures (the tendrils seen in Figure 4-9a) pulling away from the fiber surface, suggesting that the locus of failure occurs cohesively within the fiber .
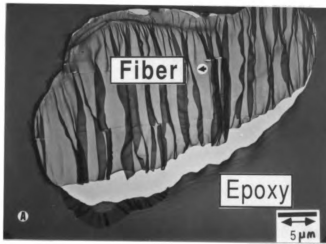
(a)
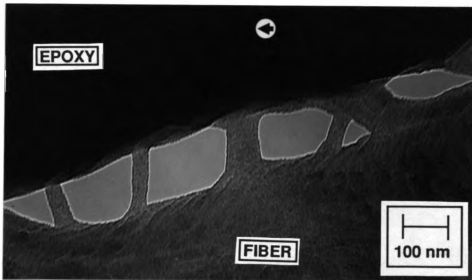
(b)

Figure 4-11: TEM micrograph of a control fiber (a) low magnification and (b) high magnification showing fibrils pulling away from fiber.

The pleated structure and occasional striations seen on the section surface indicate that microtoming conditions may have been less than optimal. Since our interest lies primarily in the fiber-matrix interface proper, the pleated structures will not affect the observed results. Figure 4-11a also indicates the highly noncylindrical nature of these fibers which varies widely from fiber to fiber and along the length of a given fiber. This varying morphology is a direct consequence of the fiber production technique as indicated by similar observations of Dyneema Sk60 polyethylene fibers.

Figure 4-12a shows a bright-field TEM micrograph of a Spectra-1000 fiber irradiated by 100 keV N^+ ions to a dose of 1×10^{15} cm^{-2}. The overall fiber matrix adhesion has improved considerably over that of the untreated fiber as evidenced by the fiber-matrix interface remaining relatively intact after the microtoming process. A higher magnification view of the fiber-matrix interface, shown in Figure 4-12b, shows the epoxy as a dark region beginning at the fiber surface and the interior of the fiber. The dark region is believed to delineate the fiber region affected by the ion irradiation and roughly corresponds to the calculated ion implantation depth of 383 nm. A smooth, sharp boundary exists between the fiber surface and the epoxy matrix region indicating a high level of fiber-matrix adhesion. Cracks produced during the microtoming are visible in the implanted region and indicate that this modified region is more brittle than the surrounding matrix and fiber. The higher contrast between the implanted region and the fiber is the result of a change in either mass or electron density from the virgin fiber. Since UHMW-PE crosslinks upon ion irradiation, both the cracking and darkness of the implanted region is evidence of the formation of a rigid 3-dimensional network and a disruption of crystallinity.

Figure 4-12b also indicates that the locus of failure shifted from the fiber-matrix interface to a point inside the virgin fiber. Separation of the fiber interior from the implanted region, with only small fibrillated structures maintaining contact, is similar to the mode of failure seen in the untreated fibers. The cohesive failure suggests that the
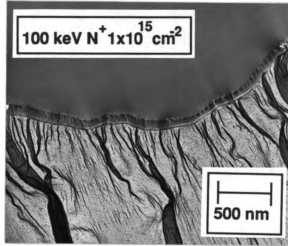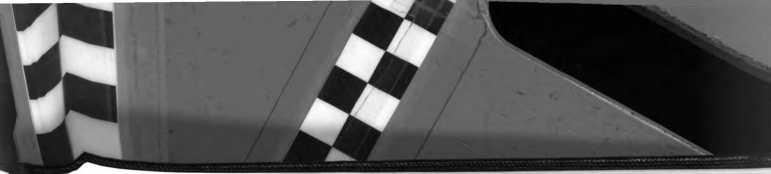
(a)
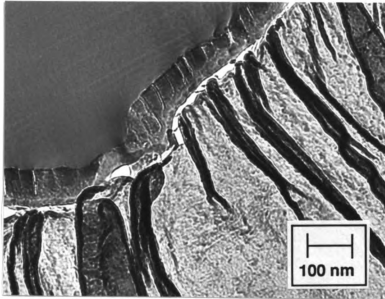
(b)

Figure 4-12: TEM micrograph of a fiber irradiated by 100 keV ions, 1×10^{15} N+/cm-2, (a) showing irradiation zone and (b) showing fibrillar decohesion.

upper limit to the fiber-matrix interfacial shear strength may be the intrinsic shear strength of the fiber itself.

Gel-Fraction of High Energy Irradiated Fibers The results of sol-gel experiments performed on 30 keV N^+ irradiated fabric as a function of dose are presented in Figure 4-13. The gel-fraction (undissovable crosslinked material) increases from a value of 0% for control to 1.24% for a dose of 1×10^{16} cm^{-2}. The small amount of crosslinked material is concentrated in the surface layers of the fiber and increases the cohesive strength of the fiber surface. The degree of crosslinking achieved probably will not affect the fiber's creep or high temperature resistance properties.
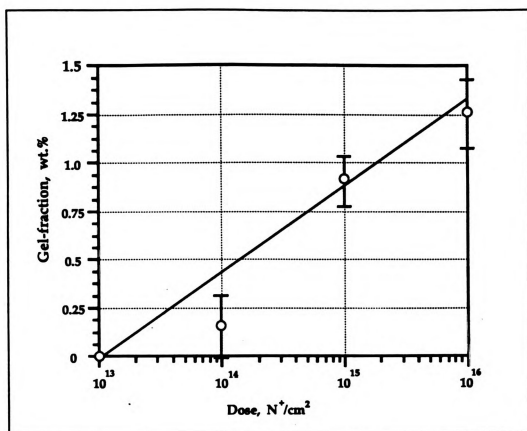
Figure 4-13: Gel-fraction as a function of dose for 30 keV N+ ions.

Low Energy Ion Irradiation of Spectra-1000

Visual Observations   Low energy ion irradiations produced a slight surface discoloration of the fabric. The most severe discoloration occurred for the 1keV, 1×10^{16} cm^{-2} irradiation's which resulted in a light brown fabric. The other processing conditions produced perceptible, but less intense discoloration. Color change is related to the amount of damage incurred by the material. These results, along with the high energy implantation results, indicate that a threshold dose (high dose regime) for discoloration exists. Since the higher energy irradiations produced more intense color changes, the ion energy is a contributing factor to irradiation induced discoloration.

Mechanical Properties   The tensile strength of 1 keV Ar$^+$ irradiated fibers as a function of dose is shown in Figure 4-14. No statistically significant decrease in strength is observed since all data points fall within the scatter band, but a slight decrease (approx. 9%) in strength from the control is evident for all doses. Figure 4-15 shows the tensile strength of Ar$^+$ irradiated fibers as a function of ion energy for a constant dose of 1×10^{16} cm^{-2}. A slight increase in strength is noted for irradiation at 100 eV, followed by a decrease to a minimum at 750 eV, and a return to near the control specimen strength (2.54 GPa) at 1 keV. The observed trends must be regarded with caution since the highly irregular cross-sectional area of Spectra 1000 fibers makes an absolute determination of the tensile strength difficult.

The normalized interfacial shear strength ($\tau_{irradiation}/\tau_{control}$) between the fiber and epoxy matrix for 1 keV Ar$^+$ irradiated fibers as a function of dose is shown in Figure 4-16. A clear trend of increasing ISS with increasing dose is observed, with the largest value of ISS being 7.75 MPa for the highest dose of 1×10^{16} cm^{-2}. This ISS value corresponds to over a 300% increase when compared to the control value of 2.41 MPa. Also indicated in Figure 4-15 are the normalized ISS values for commercial
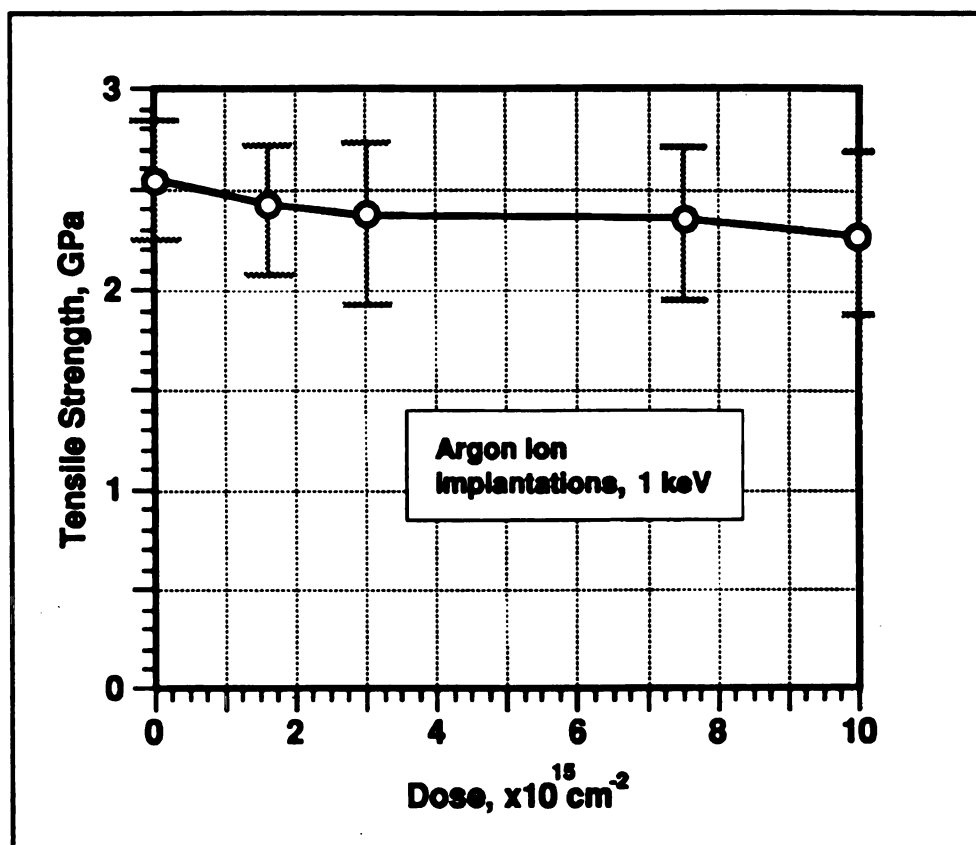
Figure 4-14: The tensile strength of 1 keV Ar$^+$ irradiated fibers as a function of dose.

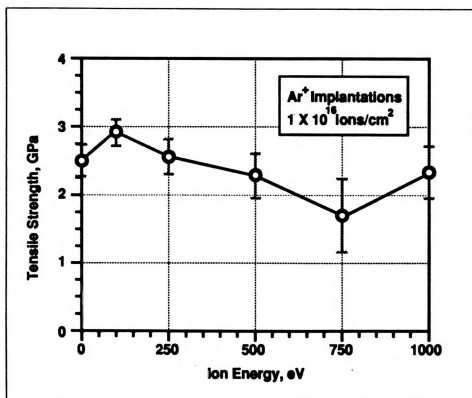Figure 4-15: The tensile strength of Ar$^+$ irradiated fibers as a function of ion energy for a constant dose of 1×10^{16} cm^{-2}.
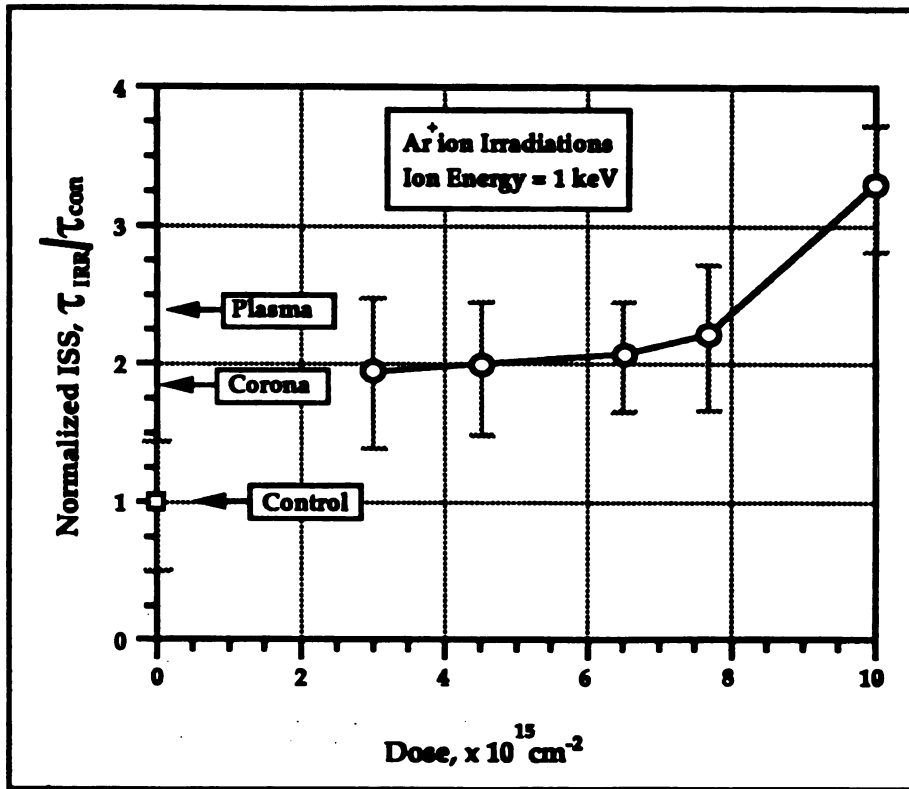
Figure 4-16: The normalized interfacial shear strength for 1 keV Ar+ irradiated fibers as a function of dose.

plasma and corona treated fibers. The corona value (4.6 MPa) is less than the plasma value (7.4 MPa) which, in turn, is slightly less than the highest ISS value. This shows that low energy ion implantation is capable of producing comparable levels of fiber-matrix adhesion comparable to those of commercial treatments.

Figure 4-17 shows the normalized ISS as a function of Ar^+ ion energy at a constant dose of 1×10^{16} cm^{-2}. Irradiation has in all cases increased ISS levels with a maximum increase of approximately 680% occurring at an ion energy of 100 eV. There is also a slight tendency for small increases in the ISS at higher implantation energies. The dose dependence of irradiation on ISS for 100 and 250 eV irradiations shown in Figure 4-18 suggests an optimum dose of 5×10^{16} cm^{-2}. At this dose, 250 eV argon ions produced a ninefold increase in interfacial shear strength level compared to the control specimens, somewhat exceeding the values for plasma and corona treatments and the values obtained by Ozzello, et al.[8] for high energy implantations (7.41 MPa, 300% increase).

Surface Chemistry   Figure 4-19 shows the oxygen:carbon ratio of UHMW-PE fabric irradiated to a dose of 1×10^{16} cm^{-2} as a function of ion energy determined by XPS. The surface oxygen concentration increases from the control value of 3.5 at.% to 15.2 at.% for the lowest ion irradiation energy of 100 eV. The surface oxygen concentration appears to be roughly constant with increasing energy, with a maximum increase of 18.2 at.% at an ion energy of 1000 eV. As in the high energy case, the source of oxygen has not been conclusively determined and could be from oxygen partial pressures in the irradiation chamber or as a result of post-irradiation exposure to atmospheric oxygen. Though N_2 was used to bleed up the vacuum chamber to atmospheric pressure, no nitrogen signal was detected. No implanted argon was observed.
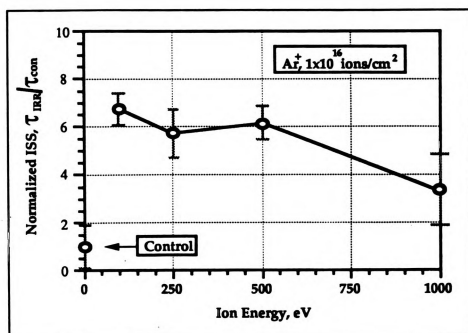
Figure 4-17: The normalized ISS as a function of Ar+ ion energy at constant dose of 1×10^{16} cm^{-2}.
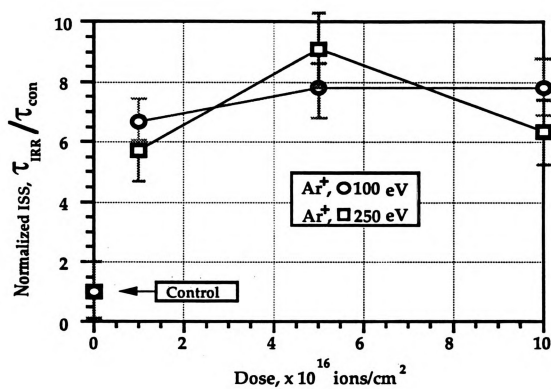
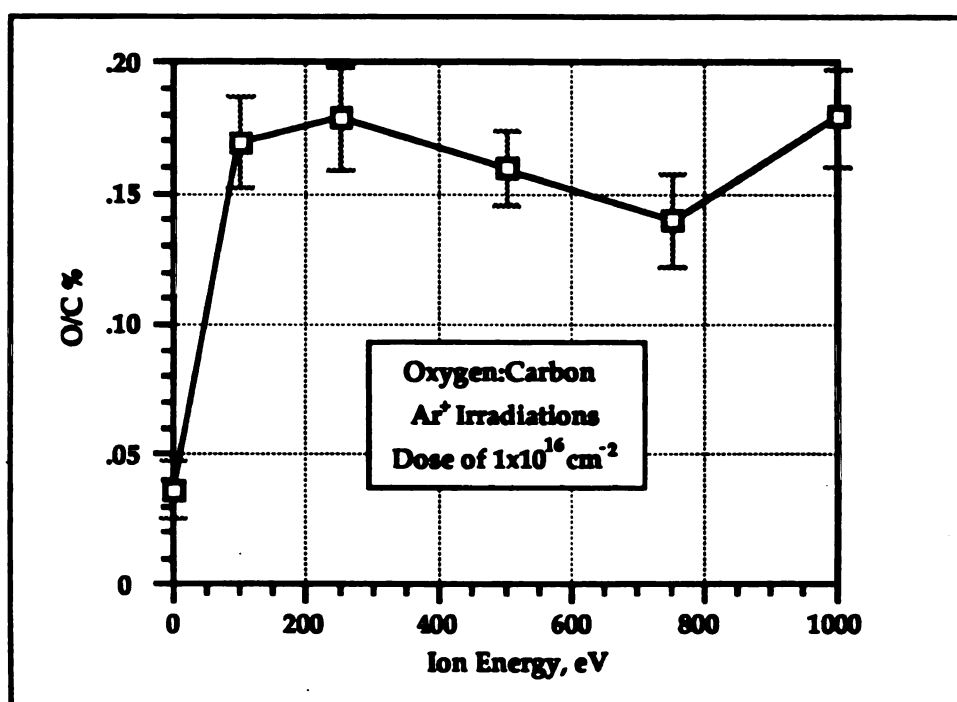Figure 4-18: The dose dependence of ISS for 100 and 250 eV Ar+ irradiations.

Figure 4-19: The oxygen:carbon ratios of fabric irradiated to a dose of 1×10^{16} cm^{-2} as a function of Ar$^+$ ion energy.

do
fur
fur
en
im
eV
lo
pe
re
re
ap
de
h

a
C
c
in
s
v
s
p

A

Figure 4-20 shows the oxygen:carbon ratio of 1 keV Ar$^+$ ions as a function of dose. The small variability (deviations less than 4 at.%) in oxygen concentration as a function of dose, suggests that a somewhat constant value is achieved. To provide further evidence for this trend, higher dose irradiations were performed at low ion energies of 100 eV and 250 eV. The oxygen:carbon ratios for the 100 and 250 eV irradiations as a function of dose are shown in Figure 4-21. For an ion energy of 250 eV, the surface oxygen concentration appears to be a maximum (17.5 at.%) at the lowest dose of 1×10^{16} cm^{-2} and then tends toward a constant value (14.0 at.%). The peak could be an indication that a free radical equilibrium concentration had been reached at a dose of 1×10^{16} cm^{-2}. For higher doses, the onset of carbonization may result in the observed decrease in surface oxidation. The data for the 100 eV ion energy appears to follow the opposite trend of increasing oxygen concentration with increasing dose. This trend suggests that 100 eV ions generate fewer free radicals, requiring higher doses to reach a peak value of oxidation.

The low energy results and the high energy results indicate that, for doses above 1×10^{15} cm^{-2}, the oxygen surface concentration is somewhat constant. Comparable levels of surface oxidation were found on the plasma (10.4 at.%) and corona (15.6 at.%) treated fibers. The ion dose, rather than energy, is therefore a more important processing parameter for the production of surface oxidation. Gerenser [65], studying oxygen plasma modified polyethylene, found a surface oxygen saturation value of approximately 20 at.%. Our study combined with Gerenser's [65] results suggests that there may be an upper limit to the amount of surface oxygen incorporation possible under certain processing conditions.

Additional information on irradiated fiber surface chemistry was obtained from ATR-FTIR measurements. Spectra for unirradiated fabric, and material irradiated with 1 keV Ar$^+$ ions and 1 keV N$^+$ ions to doses of 1×10^{16} cm^{-2} and 1×10^{15} cm^{-2}, respectively, are shown in Figure 4-22. The spectra are similar to the high energy
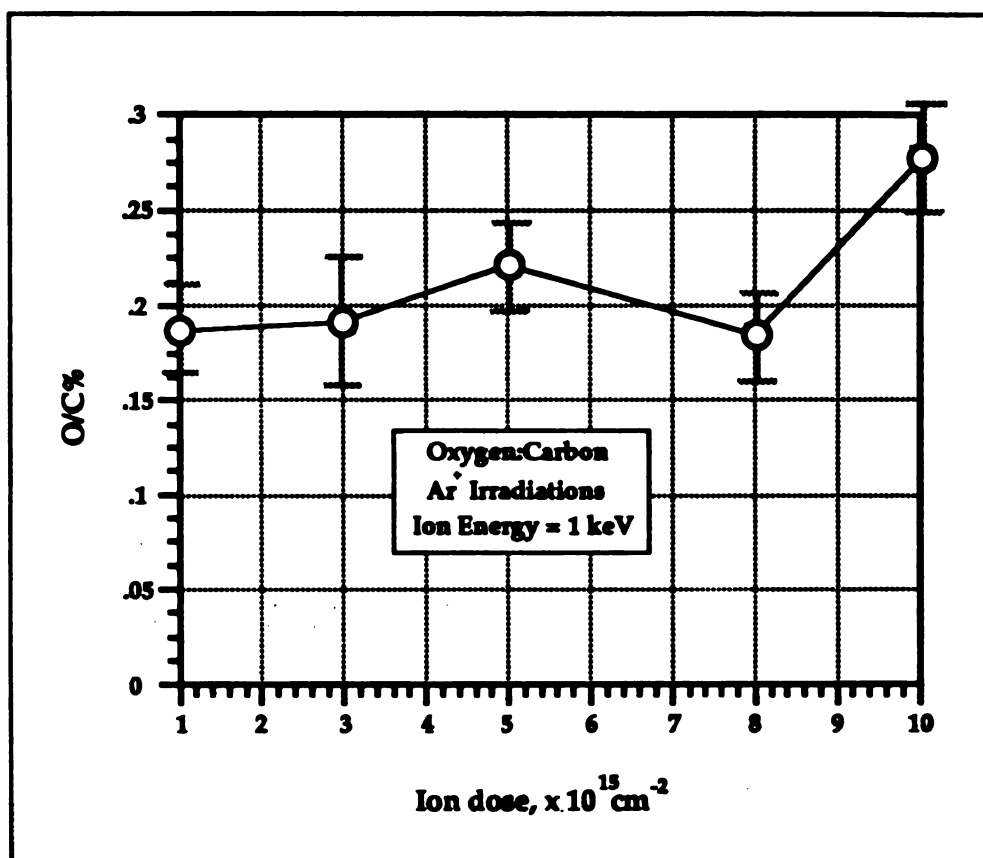
Figure 4-20: The oxygen:carbon ratios of 1 keV Ar$^+$ ions as a function of dose.
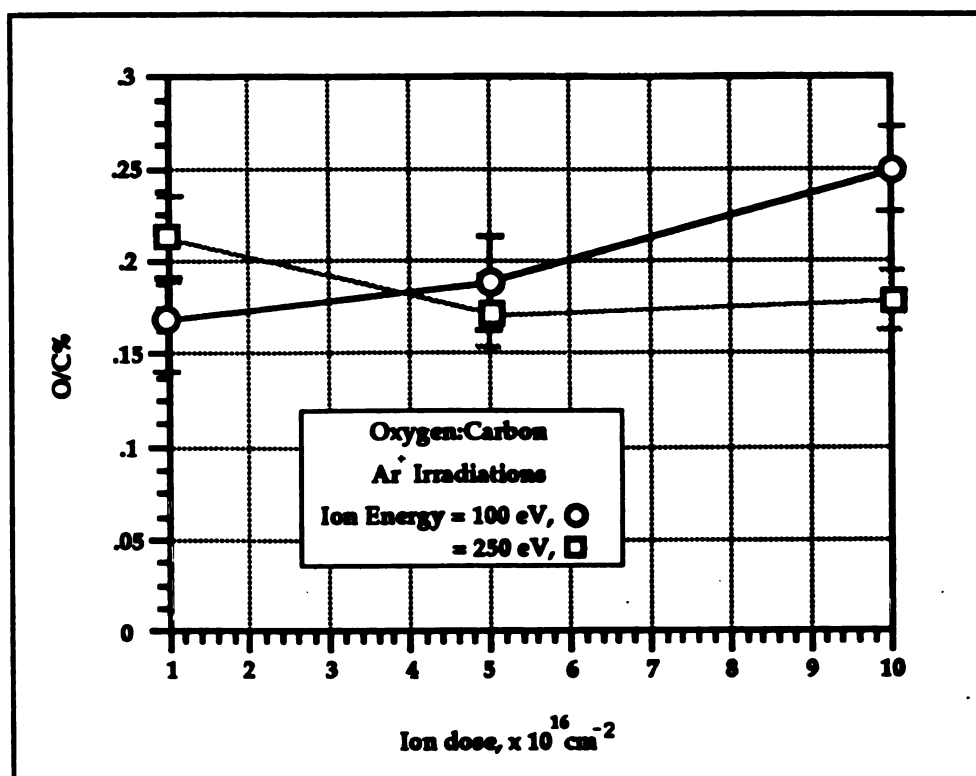
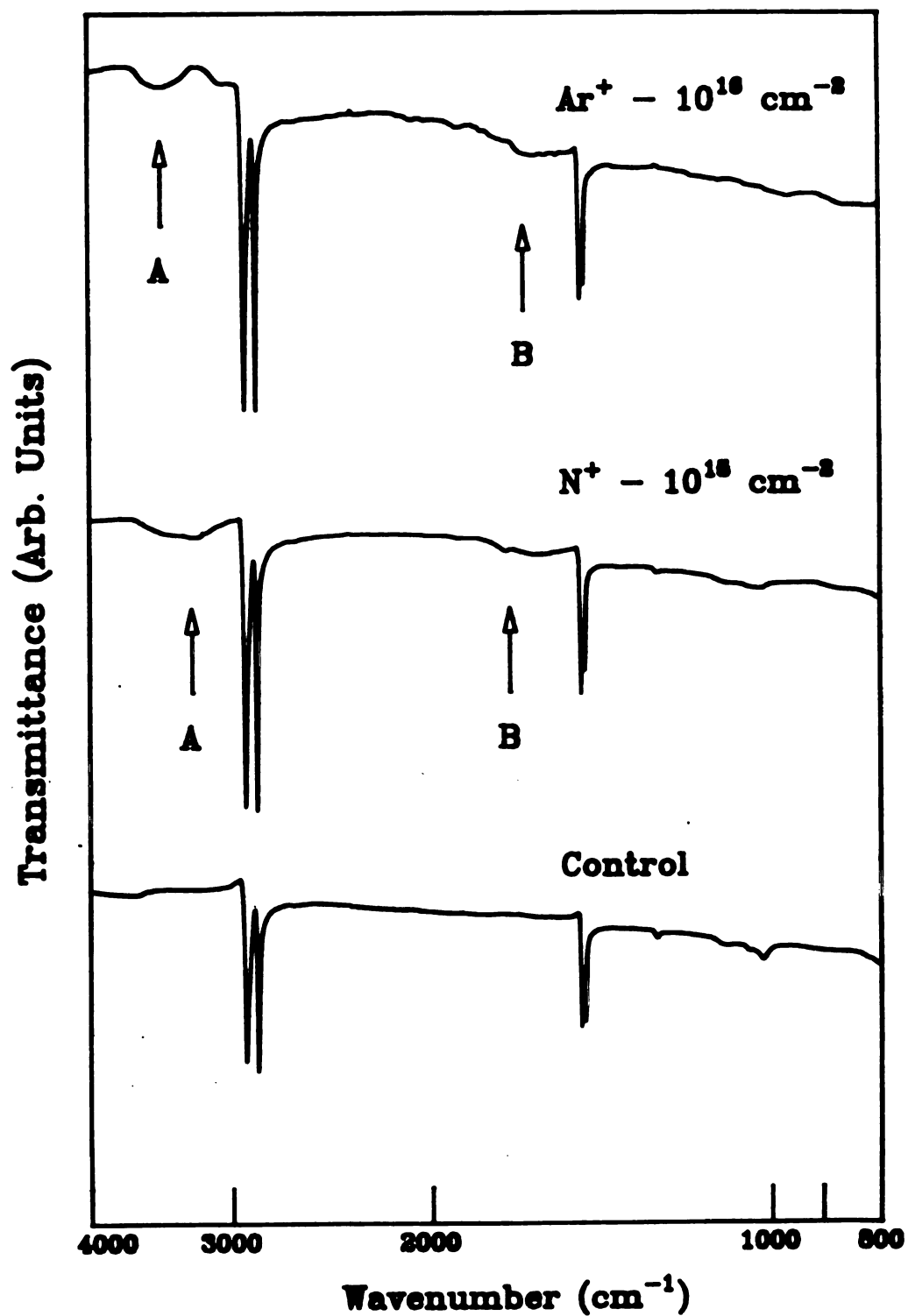Figure 4-21: The oxygen:carbon ratios for the 100 and 250 eV irradiations
as a function of dose.

Figure 4-22: Infrared spectra for fabric irradiated with 1 keV Ar+ ions and
1 keV N+ ions to doses of 1×10^{16} cm^{-2} and 1×10^{15} cm^{-2}.

spec

band

hydi

unsa

inde

larg

irra

spec

Sur

hyc

The

The

fibe

irra

slig

dis

sur

wh

= 1

im

is

fib

co

ox

spectra of Figure 4-2. In the irradiated materials, two broad composite absorption bands have developed, labeled by **A** and **B**. The **A** peak is identified as hydroxyl and hydroperoxide groups and the **B** peak contains carbonyl, carboxylic acid and unsaturated hydrocarbon [55, 60] functionalities. The functional groups generated are independent of ion species. Though the $\dot{A}r^+$ irradiation doses are an order of magnitude larger than the N^+, no distinct degradative processes (as observed in the high energy irradiations) are evident. Similar spectroscopic features were also observed for specimens irradiated at lower energies.

Surface Energy of Low Energy Irradiated Fibers   UHMW-PE fibers are hydrophobic with low surface energies which decrease with increasing draw ratio [67]. The draw ratio for Spectra-1000 fibers is greater than 30 (considered a high ratio) [68]. The total surface energy of 32 mJ/m^2 for untreated fibers causes poor wetting of the fiber by the matrix resin. Figure 4-23 plots the surface free energies of the control and irradiated fibers as a function of Ar^+ ion energy for irradiations of 1×10^{16} cm^{-2}. A slight increase in the total surface energy is observed for all ion potentials, though the dispersive component of the total energy has generally decreased. The increase in total surface energy is thus seen to be dominated by a sharp rise in the polar component, which reaches a maximum of 12.2 mJ/m^2 for the 750 eV irradiation.

For the case of Epon 828 epoxy resin the surface energy is 47.50 mJ/m^2 (polar = 10.8 mJ/m^2, dispersive = 36.7 mJ/m^2). Comparing the values found for the irradiated fibers and those of the epoxy, a closer match between the polar components is achieved, while a larger gap in the dispersive component occurs. The plasma treated fiber was found to have a total surface energy of 33.4 mJ/m^2 with polar and dispersive components of 9.4 mJ/m^2 and 24.2 mJ/m^2, respectively.

The increase in the polar component of the surface energy is a result of surface oxidation consisting of polar functional groups as identified by the IR analysis. The

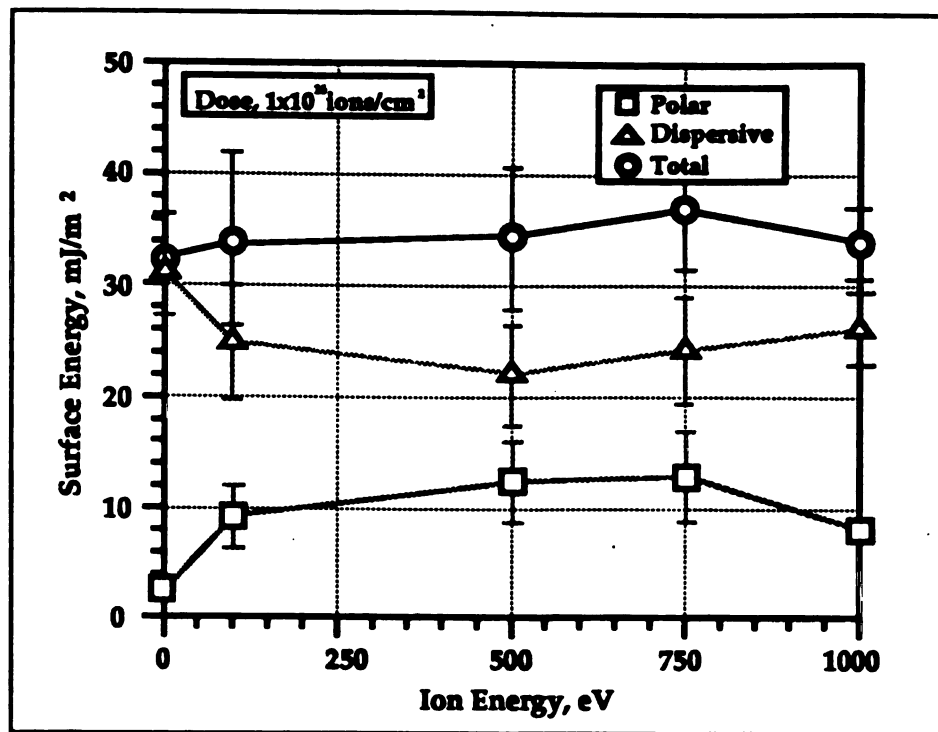Figure 4-23: The surface free energies of the control and irradiated fibers as a function of Ar^+ ion energy for irradiations of 1×10^{16} cm^{-2}.

ox

in

su

ox

fu

W

pr

ef

ar

of

pl

oc

A

m

m

re

is

st

Th

ad

di

su

m

po

oxygen-containing groups are capable of participating in strong hydrogen-bonding interactions, leading to improved wetting. The almost constant value of the polar surface energy component for the energy range examined and the somewhat constant oxidation level indicated in Figure 4-18, suggests that a constant surface density of functional groups is achieved at a dose of 1×10^{16} cm^{-2}. This also implies that the Wilhelmy method probes only the first few monolayers of the material since the projected range of 100 eV ions is 1.4 nm (~2 unit cells).

The change in the polar component of the surface energy produced a pronounced effect on the wetting properties of the fibers. Microdroplets of liquid resin readily formed and adhered to the irradiated fibers while droplets on the untreated fibers beaded up and fell off. Thus, an oxygen surface concentration of approximately 14 at.% (10 at.% if the plasma treated sample is included) provides sufficient chemical interaction for wetting to occur.

Fiber surface modification techniques tend to drive the surface far from equilibrium. All materials tend toward minimization of the surface free energy, so, ion induced surface modified properties are, in principle, time dependent. A surface modification technique must impart a stable fiber surface chemistry to be useful. Hydrophobic recovery is the reversion of a material from a hydrophilic state back to a hydrophobic state. This process is common in many polymers, including polyethylene. Though no systematic aging studies were performed, reproducible ISS results were obtained over a period of 3 months. The individual chains in UHMW-PE are rigid and make hydrophobic recovery difficult. In addition, irradiation induced crosslinking increases the rigidity of the structure, further discouraging hydrophobic recovery.

Although good wettability helps form a strong adhesive bond, it is not always sufficient for realization of increased ISS. Most commercial polyethylenes contain a low molecular weight component which, despite being perfectly miscible in the molten polymer, is ejected to the surface during processing. The high concentration of such

material on the fiber surface forms a weak boundary layer which must be removed or strengthened to achieve maximum adhesion levels. Ion irradiation may perform both functions by sputtering the low molecular weight species and crosslinking the fiber surface.

SEM Observations of Low Energy Irradiations   As discussed previously, fiber-matrix adhesion occurs through a variety of mechanisms, all of which contribute to the overall adhesion level and require investigation and characterization by an assortment of techniques. A SEM investigation of the microbond pull-out results provide phenomenological information concerning the mode(s) of interfacial failure. Figure 4-24a shows a typical debond of the microdroplet from the fiber. Note that the impressions on the droplet (B) are produced by the blades of the micrometer. The freshly exposed fiber (A) appears smooth, with longitudinal striations which indicate the presence of fibrils, and the microdroplet failure is quite symmetric about the fiber's long axis. Also, the lack of resin fragments on the fiber surface after the pull-out demonstrates that debonding is not due to cohesive failure of the matrix, but rather to sliding of the fiber along the fiber-matrix interface.

Figure 4-24b shows a droplet failure on the side opposite the blade micrometer. The matrix resin has buckled in the thin region toward the end of the droplet, again producing a more-or-less radially symmetric failure locus. Also shown, on the right hand side of the image, is an undeformed microdroplet. Here, the high degree of fiber wetting by the resin is suggested by the smooth, low angle, meniscus at the edge of the droplet which tapers out to form a thin resin film covering the entire length of the fiber. This may be compared to the meniscus of the untreated fiber, in which the contact angle is high and the thin resin film is absent, as shown in Figure 4-25. Furthermore, the embedment lengths of the microdroplets on the control fibers were, on the average, substantially shorter than those on the irradiated fibers, and axisymmetric conformation was achieved for fewer than 60% of the microdroplets applied to the untreated fibers. Axisymmetric
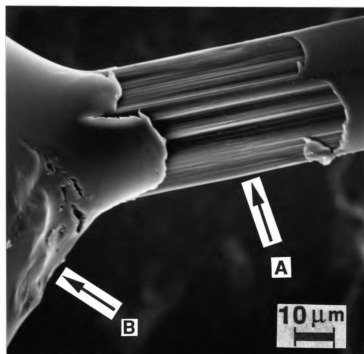
(a)
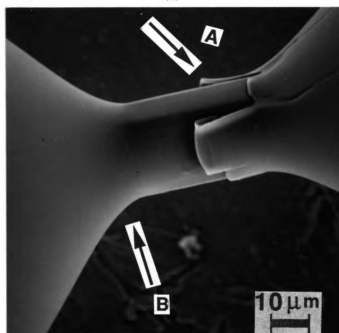
(b)

Figure 4-24: (a) Debond of the microdroplet from the fiber (note impressions made by shearing blades) and (b) droplet failure on the side opposite the blade micrometer.
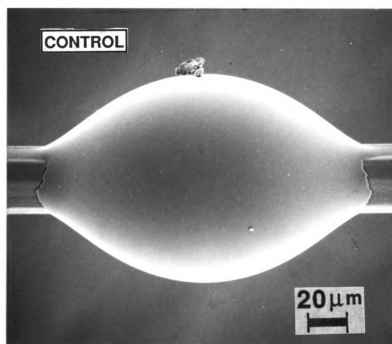
Figure 4-25: Microdroplet on untreated fiber indicating the fiber's
poor wetting properties.

conformation is known to always occur if the contact angle is low and the ratio of drop volume to fiber radius is above a critical value [69]. Failure to achieve axisymmetry is thus a further indication that wetting of the untreated fibers is inferior to that of irradiated ones.

Though most failures developed symmetrically about the fiber's long axis, occasionally cohesive failure occurs deep within the fiber, as shown in Figure 4-26. Invariably, for a given length fiber, cohesive failures (referred to as peel-off) occur for every microdroplet. Moreover, the peel-off occurs at the same fiber-matrix location for each droplet. This suggests that some fibers have an intrinsic weakness that may be related to the lamellar structure of the fiber and possibly to the spinning and drawing conditions. Similar fracture behavior is seen in melt spun polypropylene fibers [70].

Figures 4-27a and 4-27b show a comparison between the fiber morphology of UHMW-PE fibers in two irradiated conditions. A number of morphological features are present on the fiber surface after irradiating with 1 keV and 250 eV Ar^+ ions irradiated to doses of 3×10^{15} cm^{-2} and 1×10^{16} cm^{-2} respectively. First, the tendrils present before irradiation have disappeared. Secondly, blister type structures are occasionally seen on the 1 keV fiber surface. These two types of morphological structures result from thermal effects produced by the energetic ion beam and/or heat generated by the neutralizing element of the ion source. These effects are magnified by the fact that polyethylene has a low value of thermal conductivity (0.15 to 0.67 W m^{-1} K^{-1}) and low melting point, making heat transfer from the fiber surface difficult. Finally, small pits transverse to the longitudinal axis of the fiber have developed on both fiber surfaces. These pits are similar to the crack-like pits found in the plasma and corona treated fibers in Figure 4-10, but are much smaller and more uniform.

Blister type structures were observed only in the 1 keV irradiations. All lower energy irradiations had surface structures similar to the 250 eV irradiations shown in Figure 4-28b. The observed differences could be a result of irradiations at different dose rates (beam current density) and different processing times. Though the 1 keV irradiation time
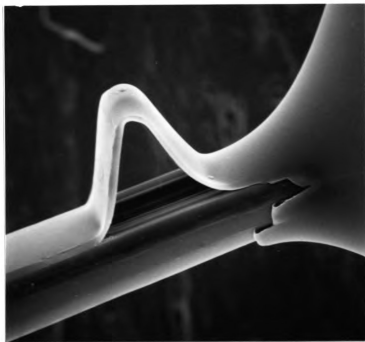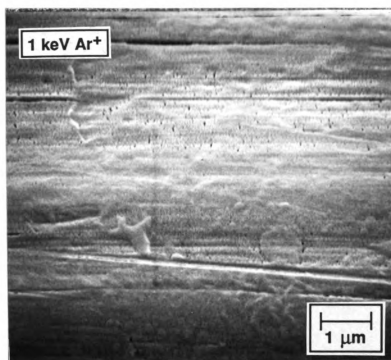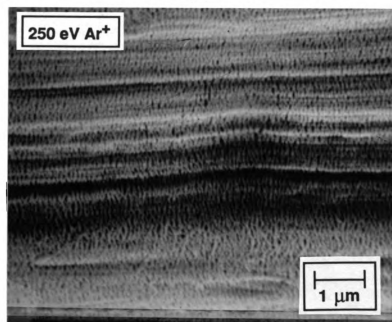
Figure 4-26: Illustration of cohesive failure occurring deep within a fiber.

(a)

(b)

Figure 4-27: SEM micrograph showing surface morphology of Ar$^+$ irradiations of
(a) 1 keV of dose 3×10^{15} cm^{-2} and (b) 250 eV of dose 1×10^{16} cm^{-2}.

(5 s) is less than the other irradiation times, the 1 keV current density (0.341 mA/cm^2) was significantly higher than the other irradiations (less than 0.267 mA/cm^2) except for the 750 eV irradiation which had a processing time of 3 sec and a current density of 0.316 mA/cm^2. The neutralizer filament current of the ion gun was kept constant during all of the irradiations and cannot be responsible for the thermal effects.

The observed morphological changes of the irradiated fiber are mostly responsible for the observed increases in interfacial shear strength. For instance, the removal of tendrils leaves tightly bound higher molecular weight species to the surface and may remove a weak boundary layer on the fiber surface. Also, the pitting encourages mechanical interlocking not previously available with the untreated fiber. Though the pits also act as stress concentrators, their effect on the tensile strength seems to be minimal. The blister type structures, however, may not be beneficial to increasing the interfacial shear strength, since they form weak surface layers on the bulk fiber and stress concentration points, which may cause premature failure. Under proper processing conditions, low energy ion implantation affects the fiber surface morphology in which ways which tend to maximize fiber-matrix adhesion.

The drawing of the fiber and high processing temperatures produce fiber surface tensile stresses upon cooldown. The fiber pitting is likely the result of the relaxation of these tensile stresses. Plasma and corona surface modification techniques many times lead to similar fiber surface morphologies, but may vary significantly for different processing parameters. The surface morphologies presented here are a representative example and are not unique. The similarities can be attributed to the similar ion dynamics occurring at the fiber surface for plasma and corona processing. The ion beam dynamics of low energy ion irradiations are well controlled and, within a certain well defined area, the ion beam is extremely uniform. The relatively high temperatures of plasma and corona processing and low energy irradiations increases the polymer chain mobility, effectively reducing the bond

breaking energy and resulting in easier stress relaxation. This type of process could easily lead to the uniform pitting observed.

Though increased surface oxidation and increased wetting of the fiber by the resin (as visually observed by ease of droplet formation) of both the plasma and corona treated fibers was achieved, the ISS values found were lower than the values reported for low energy irradiations. The fiber surface morphology of the corona and plasma treated fibers is nonuniform and may lead to complicated stress states along the fiber-matrix interface which encourages failure. The low energy irradiation produced a uniform surface texture which tends to distribute the stresses at the interface more evenly, resulting in larger ISS values. If complete wetting did not occur, voids would be produced, resulting in stress concentration sites which promote failure.

The pitting present in the previously mentioned processing methods was absent in the high energy irradiations shown in Figure 4-7. Since the high energy implantations were performed at extremely low beam currents (20μA, compared to 20 mA for low energy irradiations), thermal damage to the fiber surface is minimized, inhibiting the production of stress relaxation mechanisms. Furthermore, the high amount of energy deposition produced a substantial amount of crosslinking at the fiber surface, severely hindering stress relaxation mechanisms.

Though TRIM-91 range calculations are not strictly applicable to ion energies below a few keV, an estimate predicts ion penetrations of 5.5 nm (~7 unit cells) and 1.4 nm (~2 unit cells) at 1000 eV and 100 eV, respectively. This indicates that little subsurface modification from the kinetic effects of the accelerated ion is anticipated. A simple calculation estimates, with an assumed sputter yield of 3 atoms per ion, a conservative upper bound on the sputtered layer depth of approximately 3.5 nm. The SEM micrographs of the low energy irradiated fibers indicated morphological changes well below this depth. Thus ion irradiation not only generates free radicals, but also acts as a catalyst for fiber structural modification. The slight amount of material

removal, however, may play a significant role in ISS improvement through the elimination, or partial removal, of surface impurities and weak boundary layers.

TEM Observations of Low Energy Irradiations   To more thoroughly investigate the fiber-matrix interphase, TEM micrographs of a fiber modified by 500 eV ions with a dose of 6.0×10^{15} cm^{-2} are shown in Figures 4-27a and 4-27b. The fibers and the surrounding matrix are labeled, as is the microtoming direction. The control micrograph was previously shown in Figure 4-11 and clearly showed a low degree of adhesion between the fiber and matrix. The micrograph of the irradiated fiber indicates a well bonded fiber-matrix interphase, with decohesion occurring near the fiber's surface. A higher magnification view, shown in Figure 4-28b, of the irradiated fiber indicates failure ensues when fibrils pull away from the interface region. The same behavior was seen in fibers implanted at lower energies.

The fiber-matrix interfacial behavior for low energy ion irradiated fibers is slightly different from that of 100 keV N$^+$ irradiated fibers. In the latter, an irradiation modified region was clearly discernible and cohesive failure occurred within the fiber and not at the fiber-matrix interface proper. For the low energy irradiations, no fiber modification is detectable, but the same fibrillar breakdown at the interface is observed. Thus regardless of the type of surface modification technique, the interfacial shear occurs as cohesive failure in the fiber. The fiber surface morphology and not the intrinsic cohesive strength limits the achievable ISS. Maximum levels of ISS are therefore accomplished through adequate wetting and tailoring of the fiber surface texture for an even distribution of interfacial stresses.
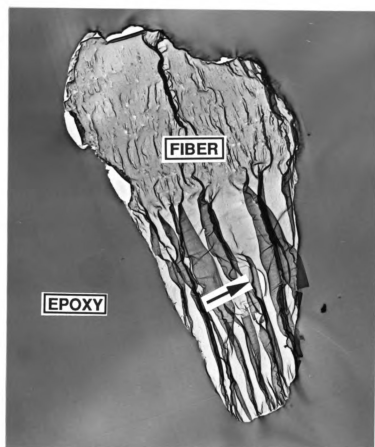
(a)
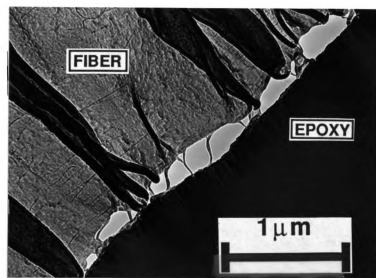
(b)

Figure 4-28: TEM micrographs of a fiber modified by 500 eV Ar$^+$ ions with a dose of 6.0×10^{15} cm^{-2}.

88

Chapter Five
CONCLUSIONS

1) High-energy ion irradiations of ultra-high molecular weight polyethylene (UHMW-PE) fibers produced surface carbonization which increased with ion dose.

2) Small decreases in tensile strength for low energy (100-1000 eV) Ar^+ ion irradiated UHMW-PE fibers were found.

3) A 900% increase in the interfacial shear strength between UHMW-PE fibers and an epoxy matrix occurred at an Ar^+ ion energy of 250 eV and a dose of 5×10^{16} cm^{-2}.

4) Low and high energy ion irradiation of UHMW-PE fibers induced surface oxidation consisting of hydroperoxide, hydroxyl and carbonyl polar functional groups.

5) The oxygen:carbon composition ratio of UHMW-PE fabric irradiated by 30 keV N^+ ions indicates a peak oxygen concentration of 16.5 at.% for a dose of 1×10^{15} cm^{-2}.

6) The gel-fraction content of 30 keV N^+ irradiated fabric increased with increasing dose.

7) Increases in the polar component of the surface free energy of low energy Ar^+ ion irradiated UHMW-PE fibers were observed at doses of 1×10^{16} cm^{-2}.

8) The fiber surface morphology of low energy Ar^+ ion irradiated UHMW-PE fibers consisted of small, uniform pits which increase the mechanical interlocking between fiber and matrix.

9) UHMW-PE fibers modified by 500 eV ions to a dose of 6×10^{15} cm^{-2} indicated a well bonded fiber-matrix interphase, with fibrillar decohesion occurring near the fiber's surface.
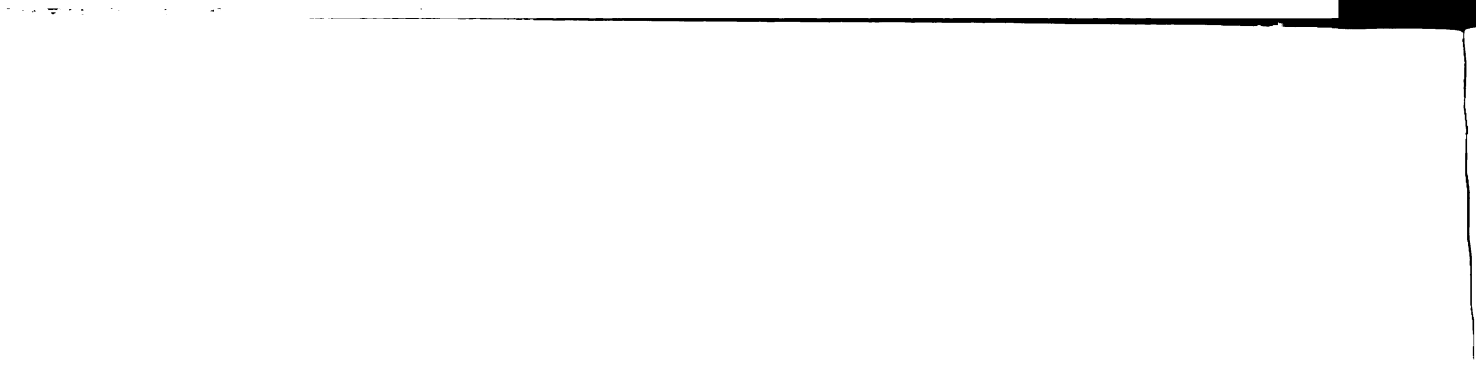
LIST OF REFERENCES

LIST OF REFERENCES

[1] L.T. Nguyen, N-H. Sung and N.P. Suh, J. Polymer Sci.: Polym. Lett. Ed. 18, 541 (1980).

[2] C. Y. Kim and D.A.I. Goring, J. Applied Polymer Sci. 15, 1357 (1971).

[3] C. Y. Kim, J. Evans and D.A.I. Goring, J. Appl. Poly. Sci. 15, 1365 (1971).

[4] S.L. Kaplan, P.W. Rose, H.X. Nguyen and H.W. Chang, SAMPE Quarterly, July, 55 (1988).

[5] J.J. Cuomo, S.M. Rossnagel and H.R. Kaufman in Handbook of Ion Beam Processing Technology: Principles, Deposition, Film Modification and Synthesis, Park Ridge, N.J. (1989).

[6] H. R. Kaufman,"Technology of Electron-Bombardment Thrusters", in Advances in Electronics and Electron Physics, 36, L. Marton Ed., pp.265-373, Academic Press, New York (1974).

[7] H.R. Kaufman, J.J. Coumo and J.M.E. Harper, J. Vac. Sci. Technol., 21, 725 (1982).

[8] A. Ozzello, D. S. Grummon, L. T. Drzal, J. Kalantar, I-H. Low and R. A. Moody, MRS Proc. 153, 217 (1989).

[9] L.T. Drzal, M.J. Rich and P.F. Lloyd, J. Adhesion, 16, 1(1982).

[10] D. Hull, An Introduction to Composite Materials, Cambridge University Press, Cambridge, England (1981).

[11] K. W. Allen, J. Adhesion, 21, 261 (1987).

[12] A. Kelly and W.R. Tyson, J. Mech. Phys. Solids, 13, 329 (1965).

[13] L.T. Drzal, M.J. Rich, J.D. Camping and W.J. Park, 35th Annual Technical Conference, Reinforced Plastics Composites Institute, The Society of Plastics

[14] L.J. Broutman, "Measurement of the Fiber-Polymer Interfacial Strength", in Interfaces in Composites, STP 452, American Society for Testing and Materials, 27 (1969).

[15] B. Miller, P. Muri and L. Rebenfeld, Composite Sci. and Technology, 28, 17 (1987).

[16] J.F. Mandell, J.-H. Chen and F.J. McGarry, Research Report R80-1, Department of Materials Science and Engineering, Massachusetts Institute of Technology, Feb. 1980.

[17] P. J. Herrera-Franco, V. Rao, M.Y.M. Chaing and L.T. Drzal, "Bond Strength Measurement in Composites -Analysis of Experimental Techniques- ",to be published.

[18] L. T. Drzal and P.J. Herrera-Franco, "Composite Fiber-Matrix Bond Tests", Engineered Materials Handbook, Vol. 3, Adhesives and Sealants, 1991.

[19] U. Gaur and B. Miller, Composites Sci. and Technology, 34, 35 (1989).

[20] G. Capaccio and I.M. Ward, Polymer Eng. Sci., 15, 219 (1975).

[21] P.J. Lemstra and R. Kirschbaum, Polymer, 26, 1372 (1985).

[22] P.J. Lemstra, R. Kirschbaum, T. Ohta and H. Yasuda, in Developments in Oreinted Polymers, Ed. I.M. Ward, Elsevier Applied Science, London (1987).

[23] D. Hofmann and E. Schulz, Polymer, Vol. 30, Nov.(1989).

[24] B. Kalb and A.J. Pennings, J. of Materials Science 15, 2584 (1980).

[25] B. Kalb and A.J. Pennings, Polymer Communications, 21, January (1980).

[26] P.J. Barham and A. Keller, Journal of Materials Science 11, 27 (1976) .

[27] E.M. Liston, J. Adhesion, 30, 199 (1989).

[28] S. Holmes and P. Schwartz, Composites Science and Technology, 38, 1 (1990).

[29] N.H. Ladizesky and I.M. Ward, J. Mat. Sci., 18 , 533 (1983).

[30] N.H. Ladizesky and I.M. Ward, J. Mat. Sci., 24, 3763 (1989).

[31] U. Gaur and T. Davidson, Mat. Res. Soc. Symp. Proc., 170, 309 (1990).

[32] B. Tissington, G. Pollard and I.M. Ward, J. Materials Science, 20, 82 (1991).

[33] H.X. Nguyen, R.G. Merrill, A.K. Schriver and E. A. Leone, Structural Composites: Design and Processing Technologies, Proceedings of the 6th Annual ASM/ESD Advanced Composites Conference, Detroit, MI, Oct. 1990.

[34] Y.L. Chen and B. Ranby, J. Polymer Sci.: Polymer Chemistry, 27, 4051 (1989).

[35] Y.L. Chen and B. Ranby, J. Polymer Sci.: Polymer Chemistry, 27, 4077 (1989).

[36] Y.L. Chen and B. Ranby, Polymers for Advanced Technologies, 1, 103 (1990).

[37] P.G. Klein, N.H. Ladizesky and I.M. Ward, J. of Polymer Science: Part B: Polymer Physics, 24, 1093 (1986).

[38] Ion implantation of Semiconductors, by G. Carter and W.A. Grant, John Wiley and Sons, New York, 1976.

[39] Ion Implantation Science and Technology, 2nd Edition, Edited by J.F. Ziegler, Academic Press, Inc., San Diego, CA, 1988.

[40] T. Venkatesan, L. Calcagno, B.S. Elman and G. Foti, "Ion Beam Effects in Organic Molecular Solids and Polymers", in Ion Beam Modification of Ionsulators, Eds. P. Mazzoldi and G.W. Arnold, Elsevier, pp.301-379, 1987.

[41] W.L. Brown, Radiation Effects, 98, 115 (1986)

[42] O. Puglisi, Materials Science and Engineering , B2, 167 (1989).

[43] D. Briggs and M.J. Hearn, Vacuum, 36, 1005 (1986).

[44] D. Briggs and M.J. Hearn, Int. J. Mass. Spect. Ion Proc., 67, 47 (1985).

[45] J. Davenas, X.L. Ku, G. Boiteux and D. Sage, Nucl. Inst. Meth., B32, 754 (1989).

[46] G. Marletta, Nucl. Inst. Meth., B46, 295 (1990).
[47] D. Fink, M. Muller, L.T. Chadderton, P.H. Cannington, R.G. Elliman and D.C. McDonald, Nucl. Inst. Meth., B32, 125 (1988).

[48] J. Davenas, G. Boiteux and M. Fallavier, Nucl. Inst. Meth., B32, 796 (1989) .

[49] S.L. Koul, I.D. Campbell, D.C. McDonald, L.T. Chadderton, D. Fink, J.P. Biersack and M. Muller, Nuclear Instruments and Methods in Physics Research, B32, 186 (1988).

[50] D. Fink, M. Muller, L.T. Chadderton, P.H. Cannington, R.G. Elliman and D.C. McDonald, Nuclear Instruments and Methods in Physics Research, B32, 125 (1988).

[51] J.F. Ziegler, J.P. Biersack and U. Littmark, The Stopping and Range of Ions In Solids, Pergamon, 1985.

[52] E.H. Lee, M.B. Lewis, P.J. Blau and L.K. Mansur, J. Mater. Res., 6, No. 3, Mar 1991.

[53] M.B. Lewis and E.H. Lee, Nuclear Instruments and Methods in Physics Research, B61, 467 (1991).

[54] A. Ishitani, K. Shoda, H. Ishida, T. Watanabe, K. Yoshida and M. Iwaki, Nuclear Instruments and Methods in Physics Research, B39, 783 (1989).

[55] M. Schaible, H. Hayden, and J. Tanaka, IEEE Transactions on Electrical Insulation Vol. E1-22 No. 6, Dec. 1987.

[56] D.H. Kaeble, P.J. Dynes and E.H. Cirlin, J. Adhesion, 6, 23 (1974).

[57] J. Kalantar, L.T. Drzal and K.J. Hook, J. Vac. Sci. Technol., A8(5), Sep/Oct, 3878 (1990).

[58] A.M. Guzuman, J.C. Carlson, J.E. Bares and P.P. Pronko, Nucl. Inst. Meth., B7/8, 468 (1985).

[59] U.W. Gedde and M. Ifwarson, Poly. Eng. Sci., 30, 4, 202 (1990).

[60] W.F. Maddams and S.F. Parker, J. Polymer Sci.: Part B: Polymer Physics, 27, 1691 (1989).

[61] M.I. Chirara and L. Georgescu, Nucl. Inst. Meth., 209/210, 401 (1983).

[62] F.A. Smidt, International Materials Reviews, 35, No 2, 61 (1990).

[63] J.A. Lanauze and D.L. Myers, J. Polymer Sci., 40, 595 (1990).

[64] H. Iwata, A. Kishida, M. Suzuki, Y. Hata and Y. Ikada, J. Polymer Sci.: Part A: Polymer Chemistry, 26, 3309 (1988).

[65] L.J. Gerenser, J. Adhesion Sci. Tech., 1(4), 303 (1987).

[66] CH. Oudet and H.H. Kausch, J. Mat. Sci. Lett.,10, 1061 (1991).

[67] M. N. and I.M. Ward, Mater. Sci. Technol., 3, 814 (1987).

[68] Personal communication, G. Weedon, Allied Signal, Petersburg, VA.

[69] B.J. Carrol, Langmuir, 2, 248 (1986).

[70] H. Bodaghi, J.E. Spuirell and J.L. White, Intern. Poly. Proc., 3 (2), 100 (1988).